

CANADIAN THESES ON MICROFICHE

I.S.B.N. 0-300-05111-1

THESES CANADIENNES SUR MICROFICHE



National Library of Canada
Collections Development Branch

Canadian Theses on
Microfiche Service

Ottawa, Canada
K1A 0N4

Bibliothèque nationale du Canada
Direction du développement des collections

Service des thèses canadiennes
sur microfiche

NOTICE

The quality of this microfiche is heavily dependent upon the quality of the original thesis submitted for microfilming. Every effort has been made to ensure the highest quality of reproduction possible.

If pages are missing, contact the university which granted the degree.

Some pages may have indistinct print especially if the original pages were typed with a poor typewriter ribbon or if the university sent us a poor photocopy.

Previously copyrighted materials (journal articles, published tests, etc.) are not filmed.

Reproduction in full or in part of this film is governed by the Canadian Copyright Act, R.S.C. 1970, c. C-30. Please read the authorization forms which accompany this thesis.

THIS DISSERTATION
HAS BEEN MICROFILMED
EXACTLY AS RECEIVED

AVIS

La qualité de cette microfiche dépend grandement de la qualité de la thèse soumise au microfilmage. Nous avons tout fait pour assurer une qualité supérieure de reproduction.

S'il manque des pages, veuillez communiquer avec l'université qui a conféré le grade.

La qualité d'impression de certaines pages peut laisser à désirer, surtout si les pages originales ont été dactylographiées à l'aide d'un ruban usé ou si l'université nous a fait parvenir une photocopie de mauvaise qualité.

Les documents qui font déjà l'objet d'un droit d'auteur (articles de revue, examens publiés, etc.) ne sont pas microfilmés.

La reproduction, même partielle, de ce microfilm est soumise à la Loi canadienne sur le droit d'auteur, SRC 1970, c. C-30. Veuillez prendre connaissance des formules d'autorisation qui accompagnent cette thèse.

LA THÈSE A ÉTÉ
MICROFILMÉE TELLE QUE
NOUS L'AVONS REÇUE

Canada

0-315-09089-X



National Library
of Canada

Bibliothèque nationale
du Canada

Canadian Theses Division

Division des thèses canadiennes

Ottawa, Canada
K1A 0N4

56926

PERMISSION TO MICROFILM — AUTORISATION DE MICROFILMER

• Please print or type — Ecrire en lettres moulees ou dactylographier

Full Name of Author — Nom complet de l'auteur

SIN-CHONG CHAN

Date of Birth — Date de naissance

NOV 1st 1949

Country of Birth — Lieu de naissance

MALAYSIA

Permanent Address — Résidence fixe

416 RANCHVIEW PLACE NW
CALGARY ALTA
T3G 1A8

Title of Thesis — Titre de la thèse

FLOW STUDIES THROUGH POROUS MEDIA USING LASER DOPPLER VELOCIMETRY

University — Université

UNIVERSITY OF ALBERTA

Degree for which thesis was presented — Grade pour lequel cette thèse fut présentée

M. Sc

Year this degree conferred — Année d'obtention de ce grade

1981

Name of Supervisor — Nom du directeur de thèse

Prof P.M. DRANCHUK

Permission is hereby granted to the NATIONAL LIBRARY OF CANADA to microfilm this thesis and to lend or sell copies of the film

The author reserves other publication rights, and neither the thesis nor extensive extracts from it may be printed or otherwise reproduced without the author's written permission.

L'autorisation est, par la présente, accordée à la BIBLIOTHÈQUE NATIONALE DU CANADA de microfilmer cette thèse et de prêter ou de vendre des exemplaires du film.

L'auteur se réserve les autres droits de publication, ni la thèse ni de longs extraits de celle-ci ne doivent être imprimés ou autrement reproduits sans l'autorisation écrite de l'auteur.

Date

JAN 25th 1983

Signature

THE UNIVERSITY OF ALBERTA

FLOW STUDIES IN POROUS MEDIA USING LASER DOPPLER VELOCIMETRY

by

(C) Sin-Chong Chan

A THESIS

SUBMITTED TO THE FACULTY OF GRADUATE STUDIES AND RESEARCH
IN PARTIAL FULFILMENT OF THE REQUIREMENTS FOR THE DEGREE
OF MASTER OF SCIENCE

IN

PETROLEUM ENGINEERING

DEPARTMENT OF MINERAL ENGINEERING

EDMONTON, ALBERTA

Fall, 1981

THE UNIVERSITY OF ALBERTA

RELEASE FORM

NAME OF AUTHOR Sin-Chong Chan
TITLE OF THESIS FLOW STUDIES IN POROUS MEDIA USING LASER
DOPPLER VELOCIMETRY
DEGREE FOR WHICH THESIS WAS PRESENTED MASTER OF SCIENCE
YEAR THIS DEGREE GRANTED Fall, 1981

Permission is hereby granted to THE UNIVERSITY OF
ALBERTA LIBRARY to reproduce single copies of this
thesis and to lend or sell such copies for private,
scholarly or scientific research purposes only.

The author reserves other publication rights, and
neither the thesis nor extensive extracts from it may
be printed or otherwise reproduced without the author's
written permission.

(SIGNED) 

PERMANENT ADDRESS:

416 RANCHVIEW PLACE N.W.
CALGARY ALBERTA
T3G 1A8

DATED 24th JUNE.....1981

THE UNIVERSITY OF ALBERTA
FACULTY OF GRADUATE STUDIES AND RESEARCH

The undersigned certify that they have read, and recommend to the Faculty of Graduate Studies and Research, for acceptance, a thesis entitled FLOW STUDIES IN POROUS MEDIA USING LASER DOPPLER VELOCIMETRY submitted by Sin-Chong Chan in partial fulfilment of the requirements for the degree of MASTER OF SCIENCE in PETROLEUM ENGINEERING

Paul Danesh

Supervisor

M. S. Elgert

E. A. M. J. J. J. J. J.

Date... 24th JUNE 1981

To
Kim and my Mother

Abstract

Experiments were performed on two simulated porous media made up of different packing arrangements of 0.5 inch lucite spheres between two lucite plates. A Newtonian oil was used as the fluid medium.

A laser doppler velocimeter was chosen to monitor the velocity in the pore space and to determine the onset of turbulence. Velocity measurements in the pore space were made by detecting the doppler frequency shift of a laser light which was scattered by contaminant particles in the oil.

The study successfully demonstrated the use of the velocimeter for interstitial velocity measurements over a range of flowrates. The results indicated that a porous medium should not be represented by a series of straight flow channels of varying cross sections. The flow geometry should include a curvilinear path of the fluid.

Acknowledgement

The author wishes to express his appreciation to Prof. P. M. Dranchuk for his supervision in this work. Thanks are also due to Prof. J. H. Masliyah for his advice which he gave so willingly.

He is also grateful to the Natural Sciences and Engineering Research Council of Canada for providing the necessary funds for this project, and to the Department of Mineral Engineering for the financial assistance.

Prof. A. W. Peterson of the Department of Civil Engineering has been most generous in the loan of the laser doppler velocimeter. Peter Steffler of the Hydraulics Laboratory has provided valuable assistance with the laser equipment. To this the author is truly grateful. The author also acknowledges Imperial Oil Ltd. for freely supplying the oils, and to the City of Edmonton for its loan of the Trident flowmeter.

Thanks are also due to the personnel of the Technical Services for their part in the construction of the cell which made the study successful. Mr. Don Sutherland of the Department of Chemical Engineering has been most helpful with the calibration of instruments and flowmeters.

Finally, a note of sincere thanks to his wife, Kim, for her patience and devotion.



Table of Contents

Chapter	Page
1. Introduction	1
2. Review of Literature	3
2.1 Flow Equations	3
2.2 Definition of Reynolds Number	5
2.3 Correlation Parameter	6
2.4 Visualization Techniques	8
3. Theory of Measurement	11
3.1 Principle	11
3.2 Mode of Operation	13
3.3 Fringe Model	14
3.4 Measuring Volume	18
3.5 Turbulent Flow	20
4. Experimental Equipment	22
4.1 Porous Medium	22
4.2 Flow System	25
4.3 Laser Equipment	29
4.4 Mounting of Cell	32
5. Procedure	34
5.1 Flowing Medium	34
5.2 Calibration	35
5.3 Alignment	36
5.4 Treatment of Data	39
6. Results	41
7. Discussion	62
8. Conclusions	70
9. Recommendations	72

Nomenclature	74
References	76
Appendix 1	81
Appendix 2	85
Appendix 3	87

List of Figures

Figure	Description	Page
1	Doppler shift	12
2	Fringe Spacing	16
3	Dimensions of Measuring Volume	19
4	Unit Cells of Packing Arrangement	23
5	Partial View of Cross Section of Cells Normal to Flow	24
6	Schematic of Flow System	27
7	Schematic of Laser Velocimetry System	30
8	Graph of ΔP vs Q - cell #1	45
9	Graph of ΔP vs Q - cell #2	46
10	Graph of ΔP vs Q - cell #2A	47
11	Velocity waveforms - cell #1	48
12	Velocity waveforms - cell #2	50
13	Velocity waveforms - cell #2A	52
14	Graph of $\Delta P/\Delta x$ vs q - cell #1	56
15	Graph of $\Delta P/\Delta x$ vs q - cell #2	57
16	Graph of $\Delta P/\Delta x$ vs q - cell #2A	58
17	Graph of C_f vs N_{rp} - cell 1 & 2	60
18	Graph of C_f vs N_{rp} - cell 2 & 2A	61
A.1	Calibration curve for Rotameter #1	93
A.2	Calibration curve for Rotameter #2	94
A.3	Calibration curve for Pressure Gauge #1	95
A.4	Calibration curve for Pressure Gauge #2	96

List of Tables

Table	Description	Page
1	Physical Properties of Packed Cells	26
2	Properties of the Oil	28
3	Components of Type 55L Laser Anemometer	31
4	Properties of Optical Intersection	42
5	Critical values at Onset of Turbulence	54
6	Characteristics of Porous Media	59
7	Comparison of Results from Cell 1	68
8	Comparison of N_r with those in literature	69

List of Plates

Plate	Description	Page
1	Optical Arrangement and Cell Mounting	33
2	View of Intersecting Beams	38
3	Oscilloscope Waveforms of Doppler Signals	55

1. Introduction

Pioneering work in the study of flow through porous media, particularly in the turbulent region, was initiated at the University of Alberta by McFarland (1). His objective was to see if the onset of turbulence in a porous medium occurred at a single value of Reynolds number. The method of streaming birefringence was used for flow visualisation. The experiment was limited in that the fluid used was non-Newtonian, and there was insufficient pressure head to create turbulence. This work is a continuation of that effort using the method of laser doppler velocimetry. Like the method of birefringence, this method is also non-intrusive. However, a Newtonian fluid can be used with this technique.

The Darcy equation has long been used for predicting the flow of fluids through porous media. It has been recognized that above a certain flowrate, the pressure drop across the medium no longer increases linearly with the flowrate, though the flow may still be laminar. The deviation from the linear relationship is due to the increasing importance of inertial effects in the porous medium. Ultimately the flow becomes turbulent as the flow velocity increases.

Throughout the literature several flow equations have been suggested to describe non-Darcy flow. Of these, the Forchheimer equation has been the most well received. It has been shown to have a mechanistic basis by Irmay (2). The Reynolds number has been commonly used to define the limits

of validity of the flow equations. This study proposes to use a Newtonian fluid and to define the upper limit of the laminar region by a Reynolds number. The second objective is to investigate if turbulent flow beyond could be described mathematically.

The measuring technique adopted for this study is laser doppler velocimetry operating in the fringe mode. The method is unique in that it is possible to obtain local fluid velocity measurement in undisturbed porous media. The velocimeter records the instantaneous velocity of tiny impurities flowing with the fluid. When these naturally occurring particles are small enough, it is reasonable to assume that they travel at the same velocity as the fluid. A profile of the local velocity provides information concerning the nature of the flow in the interstitial regions of the porous medium. Streamline or laminar flow would be indicated by a steady velocity profile over a period of time. The onset of turbulence is characterized by a continuous random fluctuation of velocity. This condition would then give rise to an unsteady velocity profile which changes with time.

2. Review of Literature

Numerous efforts have been made to understand the flow of fluids through porous media, particularly in the region where the Darcy equation is no longer applicable. Early observers attributed the non-Darcy flow to the onset of turbulence, assuming a similarity to the flow in a straight pipe. Hubbert (3) argued that comparing flow in a porous medium to that in a straight pipe is not justified as in a porous medium, non-Darcy flow appears well before turbulence sets in. This has been verified experimentally by several researchers (4,5,6,7,8)..

2.1 Flow Equations

In the case of a one dimensional, horizontal Darcy flow, the pressure gradient across the medium is directly proportional to the flowrate through it, i.e.

$$-\frac{\Delta P}{\Delta x} = \frac{\mu}{k} q \quad (1)$$

where $\frac{\Delta P}{\Delta x}$ is the pressure gradient, μ is viscosity of the fluid, k is the permeability of the the medium and q is the superficial velocity. To describe the flow beyond the Darcy region, Forchheimer (9) in 1901 presented the following two equations:

$$-\frac{\Delta P}{\Delta x} = aq + bq^2 \quad (2)$$

and

$$-\frac{\Delta P}{\Delta x} = cq^m \quad (3)$$

where a , b , c and m are constants. He suggested the use of Equation 2 as it could be reduced to the Darcy equation at low values of q . Since then Equation 2 has been called the Forchheimer equation. Other researchers (10) continued to use Equation 3 and values of m between 1 and 2 have been suggested. This equation is inadequate in that the constants do not in any way describe the physical characteristics of the porous medium. Though it is easier to fit Equation 3 on log-log paper, Trolpe et al. (11) have noted that with more reliable experimental data, a Forchheimer relation can be fitted more accurately. In general, Equation 2 is more widely accepted. It can be derived from the Navier-Stokes Equation as shown by Irmay (12) and Chywl (13). For a fully saturated homogeneous linear horizontal system, Chywl has shown that Equation 2 takes the form :

$$-\frac{\Delta P}{\Delta x} = F_a \mu q + F_b \rho q^2 \quad (4)$$

where ρ is the density of the fluid, and F_a and F_b are constants characterizing the porous medium. They are often called the viscous and inertial resistance coefficients, respectively. Comparison of Equation 4 and the Darcy equation suggests that F_a is the inverse of the permeability of the medium. Thus Equation 4 may be written as

$$-\frac{\Delta P}{\Delta x} = \frac{\mu}{k} q + F_b \rho q^2 \quad (5)$$

2.2 Definition of Reynolds Number

The Reynolds number is often used to define the limits of the validity of the various flow equations. A common form of the Reynolds number used in the literature has been

$$N_r = \frac{D \rho q}{\mu} \quad (6)$$

where D is the average particle or sphere diameter. In some cases, D has been taken to be the average diameter of the pore space. The disadvantage of using Equation 6 is that neither of the definition of D may be a characteristic length of the porous medium. Green and Duwez (14) presented

another expression which could be obtained from the definition of the Reynolds number, which is the ratio of the inertial to the viscous forces. Comparing the corresponding terms in Equation 5, the Reynolds number may be written as

$$N_{rp} = \frac{kF_b \rho q}{\mu} \quad (7)$$

This expression is preferred as it has a mechanistic base. It has been derived directly from the definition of the Reynolds number. The expression has the length parameter kF_b , which is a product of the two characteristics of the porous medium. Thus kF_b may be a better characteristic length than D .

2.3 Correlation Parameter

A typical correlation used in flow studies through pipes and porous material is the relationship between friction factor and Reynolds number. Using this correlation, Chalmers et al. obtained results similar to those obtained for coiled tubes (15). This similarity suggested to them the possibility of approximating flow through porous media to the flow through coiled pipes. Fancher and Lewis (16) plotted Fanning friction factor versus N_r and obtained a separate curve for each porous medium. They suggested that

such plots could be used to indicate the gradual change from viscous to turbulent flow taking place.

Green and Duwez (17) defined the friction factor as the ratio of 'dissipative' forces to inertial forces. Using this definition and Equation 5, the friction factor is given as

$$C_f = \frac{-\frac{\Delta P}{\Delta x}}{F_b \rho Q^2} \quad (8)$$

With the definition of N_{rp} from Equation 7, Equation 8 may then be written as

$$C_f = \frac{1}{N_{rp}} + 1 \quad (9)$$

When C_f was plotted against N_{rp} , Green and Duwez (18) showed that all the data from the various porous media fell along the curve given by Equation 9. As the choice of N_{rp} for the Reynolds number is preferred, plots of C_f versus N_{rp} will be used in this study.

2.4 Visualization Techniques

The dye tracer technique is a popular method used in many early flow studies. Among those who used it were Schneebeli (19), Chauvateau and Thirriot (20), Wegner, Karabelas and Hanratty (21) and Kyle and Perrine (22). Though the method is simple, its main disadvantage is that the coloured streamlines tend to break up after moving a short distance downstream. Furthermore, it will contaminate a closed system.

Streaming birefringence is another proven technique in flow visualisation. It is an excellent qualitative method for the study of laminar, transition and turbulent flows. McFarland (23) used this method in his studies. Unfortunately pure liquids exhibit birefringence only at very high shear rates. Flow at moderate rates would then require the use of colloidal suspensions which are non-Newtonian.

The hot-wire anemometer gained popularity in dynamic fluid studies in the 1960's. Wright (24) was one of the first to adapt the technique for use in a porous medium. Since interstitial velocity can be measured, the anemometer is useful for detecting any form of velocity fluctuation in the pore region. The onset of turbulence could then be noted. Kingston and Nunge (25) and van der Merwe and Gauvin (26) also used the hot-wire anemometer in their experiments.

The main disadvantage of hot-wire anemometry is that the technique is intrusive. Its very presence alters the

conditions in the flow stream. The hot-wire can be made very small. It is very fragile and has to be carefully inserted in the pore space.

Laser doppler velocimetry appears to be an attractive technique for quantitative flow studies especially in the turbulent region. The phenomenon of doppler frequency shift has been known for many years. It was not until 1964 when Yeh and Cummins (27) successfully demonstrated the application of laser doppler velocimetry. They conducted measurement of a steady laminar flow of water in a pipe using a He-Ne laser. Their success prompted others to use the technique (28,29,30). Goldstein and Kreid (31) reported accuracy of measurement of 0.1%. Measurements in the turbulent region were first made by Goldstein and Hagan (32) in 1967.

This technique proved popular and by the early 1970's, complete commercial packages were available for velocity measurement (33). The main advantage of this method is that it is non-intrusive and thus does not perturb the flow. It also records velocity directly and requires no calibration (34). However, in this method the medium must be optically transparent to the laser beam. There must be sufficient scattering particles in the fluid to cause a strong doppler signal. In some cases, these scattering particles may have to be introduced into the fluid.

To date, only one study of flow in a porous medium using a laser doppler velocimeter has been reported. In

1974, Johnston et. al. (35) measured velocities in the interstitial regions of a packed cell made up of transparent Plexiglas spheres. The fluid used had a refractive index close to that of the glass spheres at the wavelength of the laser beam. The investigation demonstrated that a laser velocimeter could be used for flow measurements in a porous medium.

3. Theory of Measurement

3.1 Principle

A laser doppler velocimeter is an optical flowmeter. The light beam from a laser source is scattered by particles moving with the flowing fluid. A doppler frequency shift occurs and it is defined as

$$f_d = f_s - f_i \quad (10)$$

where f_s and f_i are the frequencies of the scattered and incident beams, respectively. Written in terms of the velocity of the moving particle, Equation 10 has been shown by Watrasiewicz and Rudd (36) to be

$$f_d = \frac{U}{\lambda} \cdot (\hat{e}_s - \hat{e}_i) \quad (11)$$

where U is the velocity of the particle, λ is the wavelength of the incident beam, \hat{e}_s and \hat{e}_i are the unit vectors of the scattered and incident beams, respectively. From Figure 1, it can be deduced that the velocity component measured is in the direction $(\hat{e}_s - \hat{e}_i)$. The magnitude of $(\hat{e}_s - \hat{e}_i)$ can

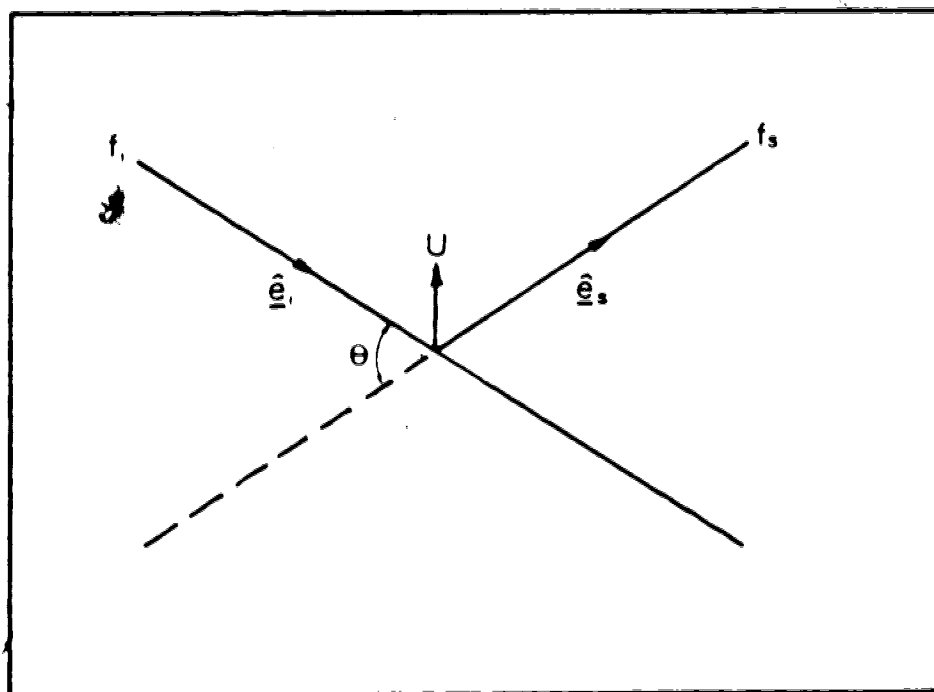


Fig.1 DOPPLER SHIFT

be shown to be $2 \cdot \sin(\theta/2)$, where θ is the angle through which the incident beam has been scattered. Rewriting Equation 11 in terms of the velocity gives

$$f_d = \frac{U \cdot 2 \cdot \sin\theta/2}{\lambda} \quad (12)$$

Equation 12 shows that the doppler shift f_d is directly proportional to the velocity of the particle. The small particle is assumed to have the same velocity as the flowing fluid.

The variation of velocity of flow, given by Equation 12, would with time indicate the kind of flow behaviour taking place in the region under study. A constant velocity is characteristic of streamline or laminar flow. A velocity profile randomly fluctuating with time would indicate turbulent flow. The transition between the laminar and turbulent regimes has sometimes been referred to as a period of intermittent flow. In this region, the flow alternates between the laminar and the turbulent states (37).

3.2 Mode of Operation

Several optical arrangements are available for laser doppler velocimeters. They are the ; (1) Reference Beam mode (2) Differential Doppler mode and (3) Dual Scatter Mode. A

description of these modes of operation is given by Durst et al. (38) and Watrasiewicz and Rudd (39). They are generally described in terms of the doppler effect. However, in 1969, Rudd (40) proposed an alternative model which gives a good visual description of the system. He described the effect in terms of a fringe pattern, thus the name, fringe model.

3.3 Fringe Model

A beam splitter placed in front of the laser unit produces two coherent monochromatic laser beams. When these two beams interfere, they form a set of dark and bright fringes in the intersecting volume. The spacing between the alternate bright fringes (41) is given as

$$\Delta s = \frac{\lambda}{2 \cdot \sin \theta / 2} \quad (13)$$

A particle moving across the interference fringes with a velocity component perpendicular to the fringe planes will vary the light intensity of the fringe pattern. When observed from any direction, this variation is in the form of a sinusoidal intensity fluctuation. A photomultiplier is used to detect this fluctuation. The output of the photomultiplier is an electrical signal having a frequency dependent upon the velocity of the particle moving across

the fringe pattern (See Figure 2). The frequency of light variation may be written as

$$f_m = \frac{1}{\Delta t} \quad (14)$$

where Δt is the time to cross one fringe spacing. It may be written as

$$\Delta t = \frac{\Delta s}{U} = \frac{\lambda / (2 \cdot \sin \theta / 2)}{U} \quad (15)$$

Therefore

$$f_m = \frac{U \cdot 2 \cdot \sin \theta / 2}{\lambda} \quad (16)$$

Equation 16 is identical to Equation 12 obtained from the doppler shift consideration.

For measurement in a liquid, Equation 16 becomes

$$f_m = \frac{U \cdot 2 \cdot \sin \theta_l / 2}{\lambda_l} \quad (17)$$

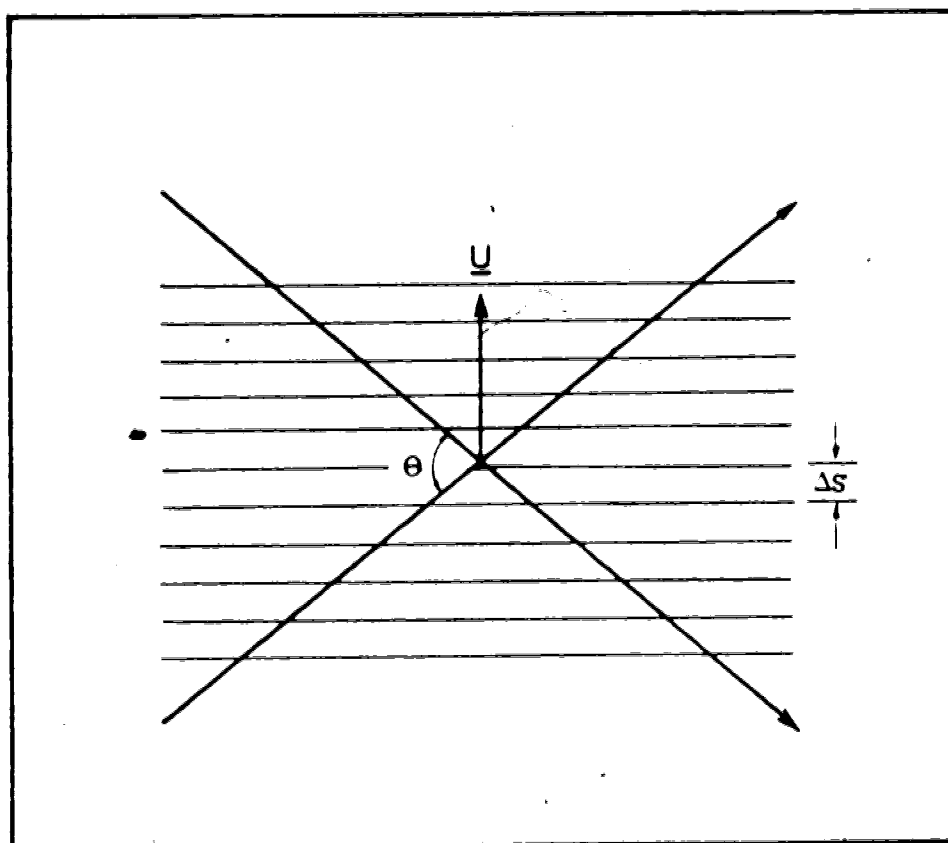


Fig. 2 FRINGE SPACING

where θ_ℓ is the angle between the intersecting beams and λ_ℓ is the wavelength in the liquid. From the definition of refractive index and the laws of refraction, Longhurst (42) showed that

$$\frac{\lambda_\ell}{n} = \frac{\lambda}{n_\ell} \quad (18)$$

and

$$n_\ell \sin(\theta_\ell/2) = n \sin(\theta/2) \quad (19)$$

where n_ℓ is the refractive index of the fluid. Therefore

$$\sin(\theta_\ell/2) = \frac{n}{n_\ell} \sin(\theta/2) \quad (20)$$

or

$$\frac{\sin(\theta_\ell/2)}{\lambda_\ell} = \frac{\sin(\theta/2)}{\lambda} \quad (21)$$

Substituting Equation 21 into Equation 17 gives Equation 16. Thus Equation 16 is also valid for measurement in liquid provided the proper values of θ and λ are used.

3.4 Measuring Volume

The volume formed by the two intersecting beams, sometimes called the measuring or control volume, is an important parameter in the velocimetry system. It defines the spatial resolution of the system.

The beam intersecting angle, θ , is calculated from the geometry formed by the two beams leaving the beam splitter (See Appendix 1). From a consideration of the Gaussian properties of the light beams and the optics of the converging lens, the dimensions of the measuring volume, as indicated in Figure 3, has been shown (43) to be

$$w = \frac{4}{\pi} \cdot \frac{(\lambda)(f)}{D_e} \cdot \frac{1}{\sin\theta/2} \quad (22)$$

$$d = \frac{4}{\pi} \cdot \frac{(\lambda)(f)}{D_e} \cdot \frac{1}{\cos\theta/2} \quad (23)$$

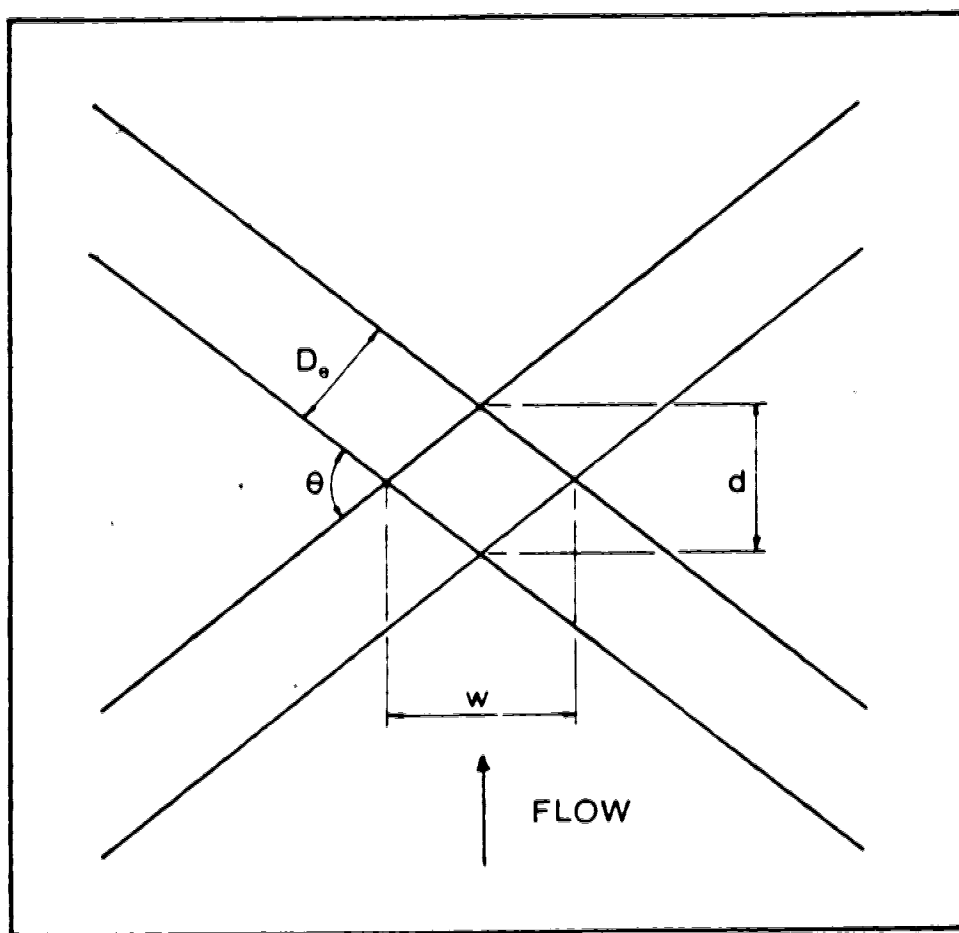


Fig.3 DIMENSIONS OF MEASURING VOLUME

where f is the focal length of the converging lens and D_e is the beam diameter. Using Equations 13 and 23, the number of fringes in the measuring volume may be estimated as

$$N_{fr} = \frac{d}{\Delta s} \quad (24)$$

3.5 Turbulent Flow

The instantaneous velocity at any point in the flow may be written in the form

$$U = U_m + u \quad (25)$$

where U_m is the time averaged mean velocity and u is the fluctuation about the mean. For steady laminar flow, there is no fluctuation of velocity and so $u = 0$ (44) and U and U_m are equal. In turbulent flow, there is a fluctuation of the instantaneous velocity about the mean U_m . However, the time averaged value of this fluctuation, u is 0. As mentioned earlier, the intermittent region is characterized by alternating periods of laminar and turbulent flow. The fraction of time during which turbulence occurs at a given

position is defined by Schlichting (45) as the intermittency factor, γ . Thus $\gamma = 0$ defines the flow as laminar and $\gamma = 1$ corresponds to the onset of turbulence. During the period of intermittent flow, γ has a value greater than 0 and less than 1.

4. Experimental Equipment

4.1 Porous Medium

To simulate porous media, packed cells of different flow geometry were used. It was originally intended that all the 4 cells from McFarland's work (46) were to be tested in this study. However, only two of the cells could be located. After some preliminary runs, it was found that only one of them had pore spaces large enough to accommodate the two intersecting laser beams without reflection from the sides of the spheres. This was the Cubic No. 1 cell with spheres of 0.50 ± 0.01 inch diameter. The stainless steel ball bearings were replaced by lucite spheres. Another cell of a different pack was constructed. It will be referred to as the Cubic No. 2 cell. It has the same size spheres as Cubic No. 1. The cubic unit cell is similar to that in Cubic No. 1 except that it has been rotated through 45° about one of its edges. The two packing arrangements are illustrated in Figure 4 and Figure 5.

Each pack consisted of two layers of spheres between 1 inch thick lucite plates. The spheres in each layer were recessed to half their diameters into each lucite plate to reduce wall effects. Each recess in the lucite was made with the aid of a programmable drill press, producing a grid of holes of centres 0.50 ± 0.005 inch apart. Both cells had arrays of 10 rows by 27 columns of spheres. Each cell had an

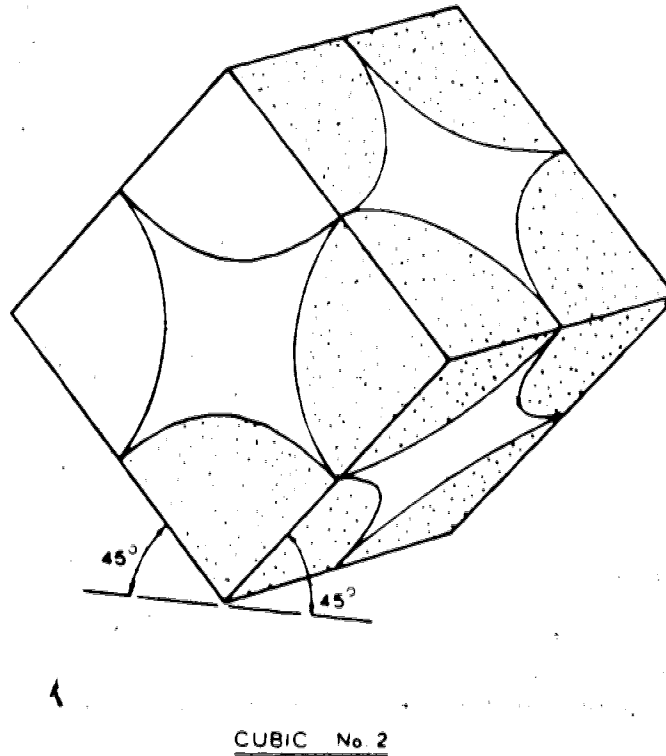
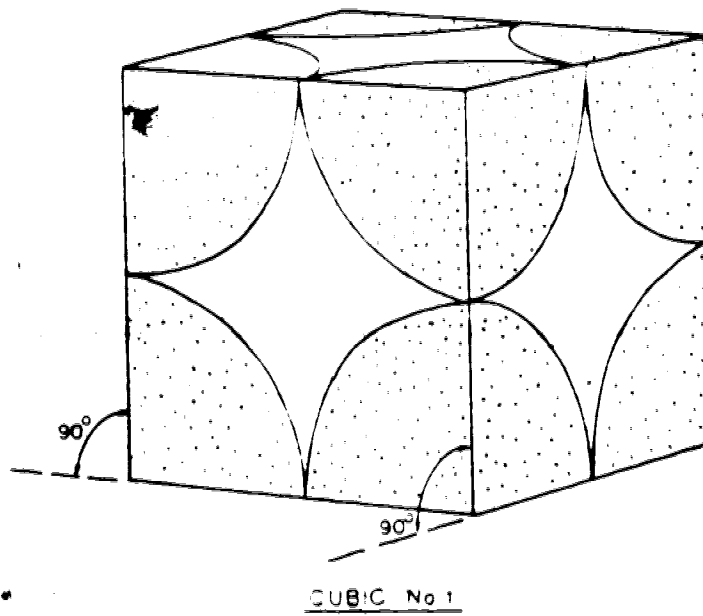
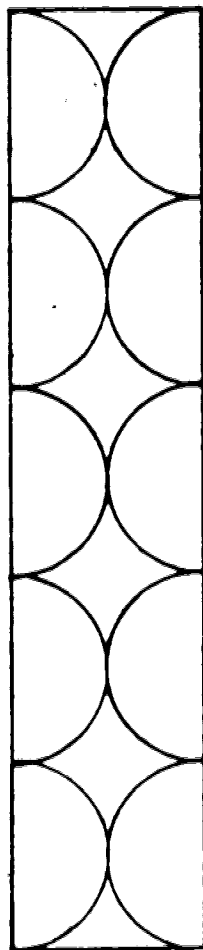
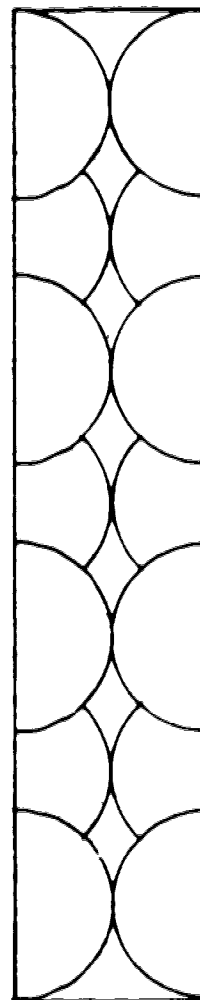


Fig.4 UNIT CELLS OF PACKING ARRANGEMENT



CUBIC No. 1



CUBIC No. 2

Fig. 5 VIEW OF PARTIAL CROSS SECTION OF CELLS
NORMAL TO FLOW

inlet flow diffuser to minimize flow perturbation. Pressure taps were located eight sphere columns downstream of the inlet and four sphere columns upstream of the outlet. The physical properties of each cell are presented in Table 1.

4.2 Flow System

In order to obtain a constant pressure head sufficient to cause turbulent flow, oil was gravity-fed from a tank on the eighth floor of the Chemical-Mineral Engineering building. A schematic of the flow system is illustrated in Figure 6. A continual overflow was provided at the upper tank to maintain the constant head of pressure. A 45-meter head was available at the basement of the same building. It was a closed system with a centrifugal pump to return the oil to the upper tank. The pump used was an Aurora Turbine pump driven by a single-phase 1.5 hp motor. The plumbing consisted mainly of PVC components. The two tanks were made of polyethylene. The properties of the oil used in the system are shown in Table 2.

An inlet manifold was designed such that three flowmeters were connected in parallel, each having its own control valve. Two of the meters were Rotameters while the third was a Trident volumetric flowmeter. Depending on the flowrate, the two Rotameters could be used in parallel.

The two pressure taps of the cells were connected to a Validyne differential pressure transducer. Two diaphragms of

Table 1. Physical Properties of Packed Cells

Cell # No.	D (cm)	A (cm ²)	ΔX (cm)
1	1.27	16.42	20.38
2	1.27	11.88	12.60

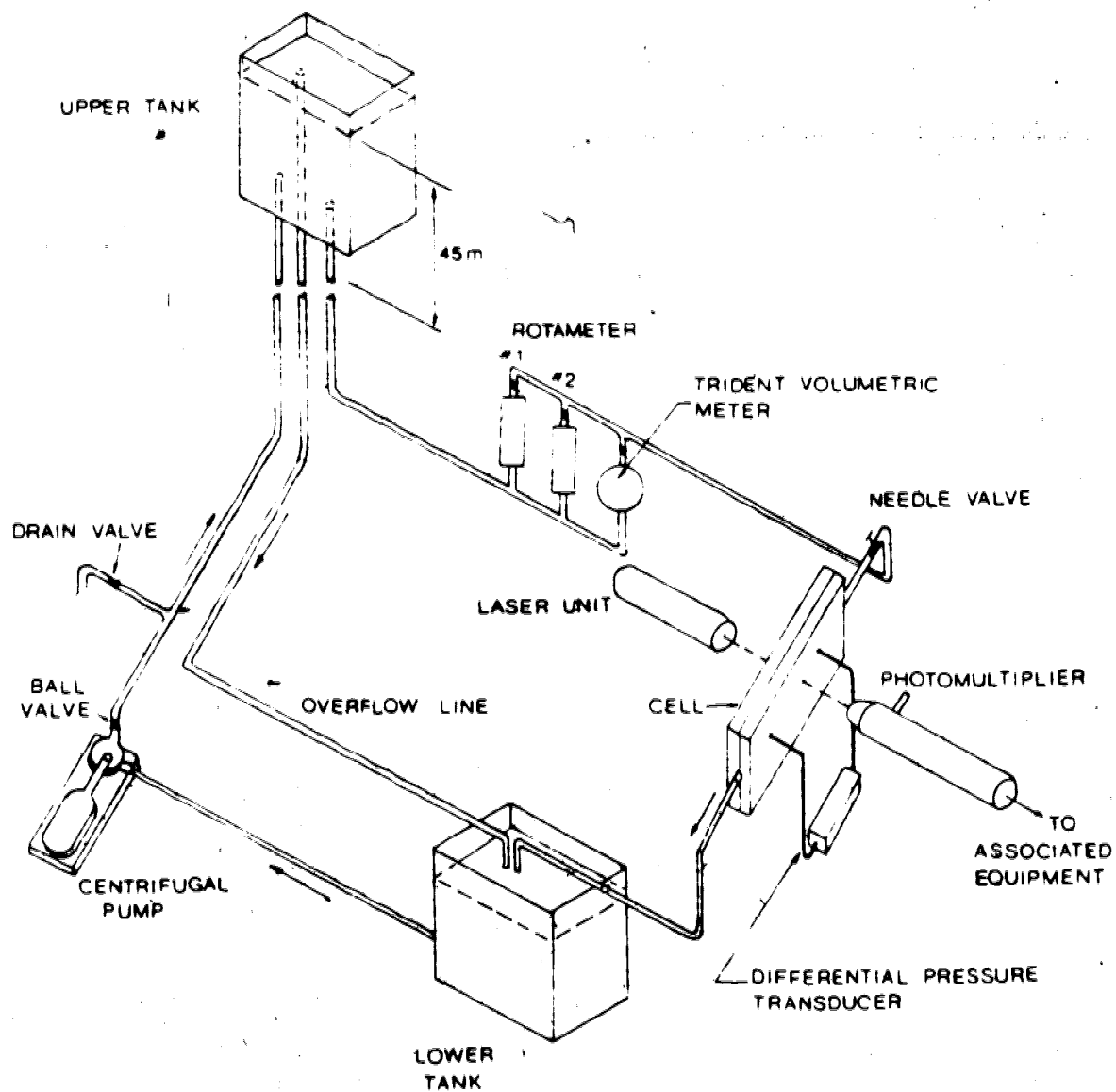


Fig. 6 SCHEMATIC OF FLOW SYSTEM

Table 2. Properties of the Oil at $29.0^{\circ} \pm 1.0^{\circ}\text{C}$.

Viscosity 16.4 mPa.s

Density 850.1 kg/m^3

maximum rating of 6.89 kPa (1.0 psi) and 0.69 kPa (0.1 psi) respectively were available. The sensitivity of the system was 1 % of the maximum rating of the diaphragm. This arrangement measured the pressure drop across the two taps.

4.3 Laser Equipment

The velocimetry system employed in this study used the fringe mode with forward scatter. The laser and its associated equipment are illustrated in Figure 7. The He-Ne laser unit, Spectra Physics (Model 120), produces 5 mW of continuous luminous radiation of a wavelength of 6328 Å. The Optical Unit split the incoming beam into two beams which intersected in the region of interest. The light scattered by the moving fluid was detected by the photomultiplier. An oscilloscope was necessary to monitor the presence of a doppler signal. For this purpose the Hewlett Packard 564 was used. The doppler frequency signal was then processed and displayed. The display could either be in the form of a direct frequency read-out from a meter or a trace on an X-Y recorder. In the latter, the root-mean-square value of the voltage represented the fluctuation of the measured velocity about the mean. The velocimeter used in this study is the Type 55L Laser Doppler Anemometer from Disa Electronics. The components of the package are listed in Table 3.

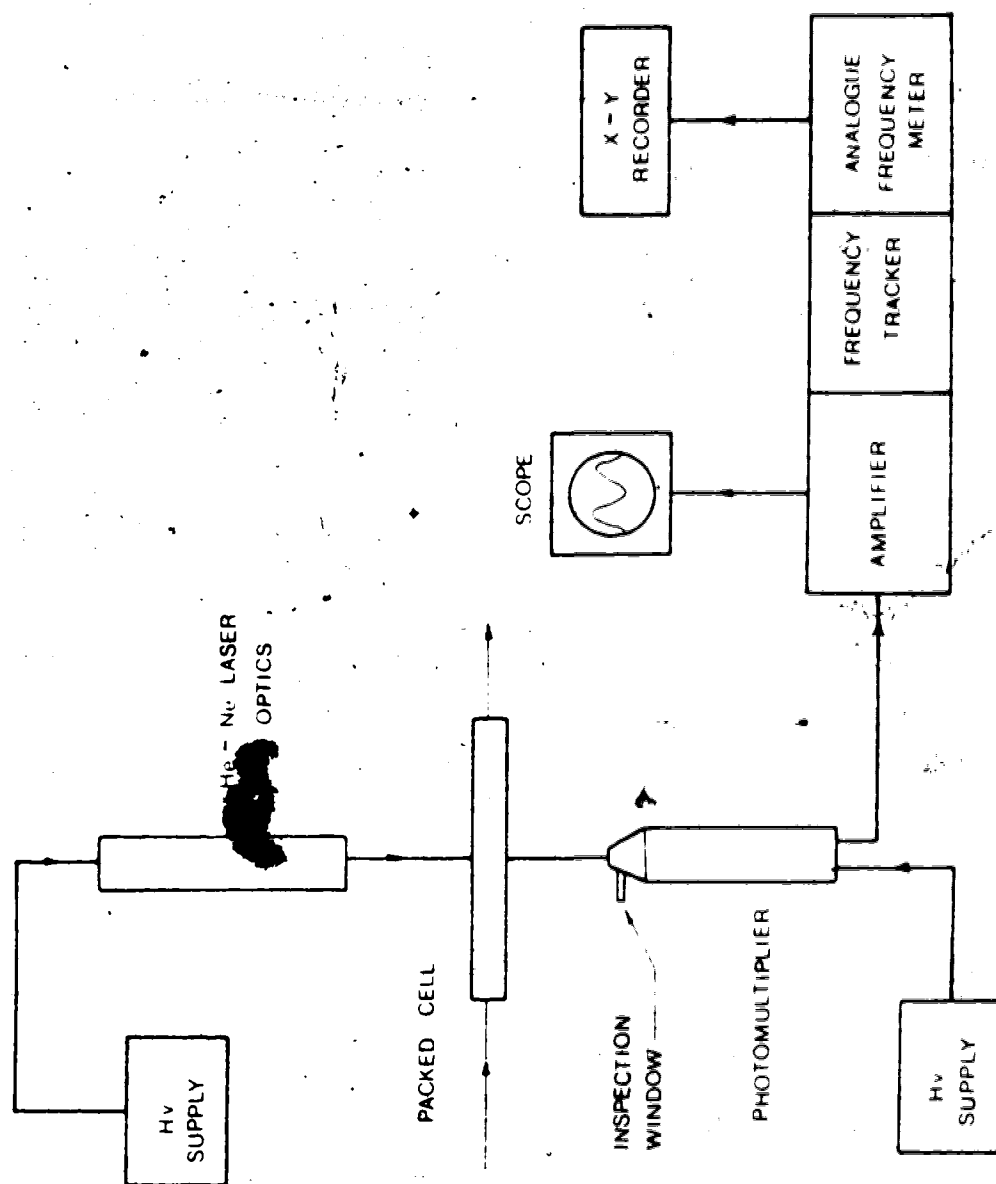


Fig. 7 LASER VELOCIMETRY SYSTEM

Table 3. Components of Type 55L Laser Doppler Anemometer

Laser Unit	Spectral Physics Model 120
Optical Unit	Type 55L01
Photomultiplier	Type 55L10
PM Tube	EMI Type 96588
HV Supply	Type 55L15
Signal Processor	Type 55L20

4.4 Mounting of Cell

As Goldstein and Kreid (47) had observed, it was more convenient to have the test cell mounted on a moveable platform. This allowed different pore sections to be examined without upsetting the laser and the photomultiplier tube alignment. For this purpose, a milling machine was used on which the cell rested on a steel plate placed on three pneumatic dampers. The milling table was restricted to movement in the plane normal to the direction of the laser beams. Both the laser and optical units rode on an optical bench on one side of the cell. The photomultiplier and the processing electronics were on the other side of the cell. Plate 1 shows a view of the optical arrangement and the mounting of the cell.

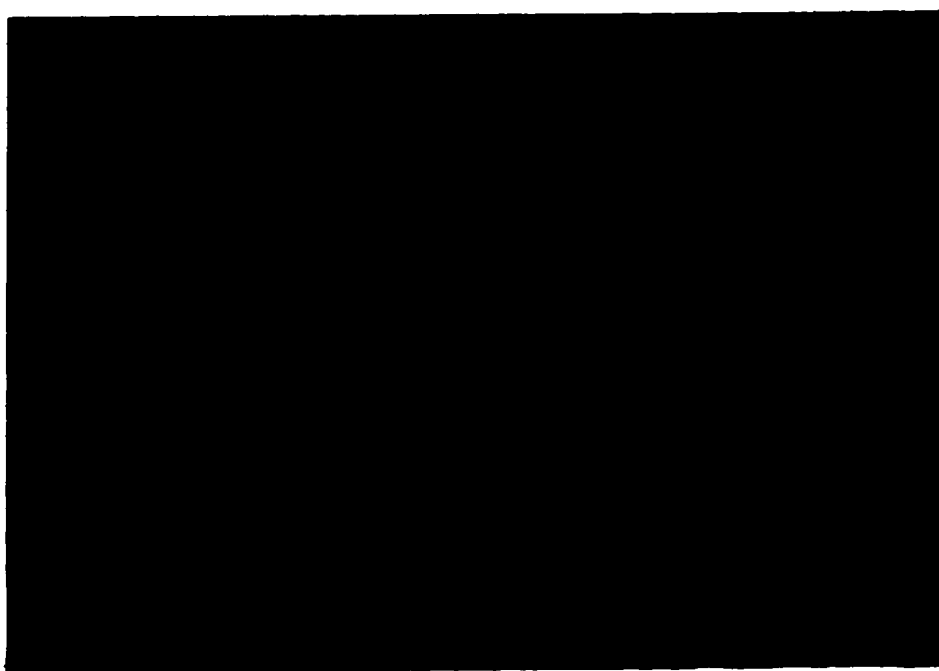


PLATE 1. OPTICAL ARRANGEMENT AND CELL MOUNTING

5. Procedure

5.1 Flowing Medium

Initial tests were carried out using tap water as the flowing medium. The pressure drop across the measuring points was too low to be recorded by the differential pressure transducer. The flowing medium was then changed to a blend of two oils. Uniflo Base Oil and Light Atmospheric Gas Oil were mixed in a proportion of about 3 to 2 by volume. The Newtonian nature of the mixture was verified on a Weissenberg Rheogoniometer. It was unnecessary to seed the oil as there were sufficient scatterers in the system to provide good doppler signals.

It was observed during preliminary runs that the oil flowing through the system reached a steady temperature of $29.0 (\pm 1.0) ^\circ\text{C}$. All subsequent observation and measurement of properties were made at that temperature.

The properties of the oil are given in Table 2. The viscosity of the oil was measured with the aid of a Cannon-Fenske viscometer in a bath kept at 29.0°C . The oil density was determined using a density bottle.

5.2 Calibration

The Rotameters were calibrated by collecting volumes of oil passing through in a given period of time. The amount of oil collected was weighed. Calibration graphs of mass flowrate versus Rotameter reading were then obtained. These are presented in Figures A.1 and A.2.

The Trident volumetric flow meter was checked for its accuracy. A volume of 0.20 cu. ft. of oil as recorded on the meter was collected and weighed. The volume of the amount of oil collected was then calculated from its density and weight. The mean value was found to be 5670 ± 10 cc. The flowrate could then be calculated by recording the time taken for 0.20 cu. ft. (meter reading) of oil to pass through the meter.

The Validyne differential pressure transducers were calibrated in the Standards Laboratory of the Department of Chemical Engineering. The associated equipment consisted of a demodulator and a digital voltmeter. Transducer 2 could not be calibrated for pressure differences less than 0.19 kPa. The regulator valve used in the Standards Laboratory could not be finely controlled at those low values. The calibration graphs of the two transducers are found in Figures A.3 and A.4.

5.3 Alignment

Prior to any optical alignment, the tables on which the laser unit and the packed cell were to be placed were isolated from the floor to minimize building vibration.

The beam from the laser was made to pass through a beam splitter. The two beams were then aligned to ensure that they intersected at the focal point of the convex lens of 13 cm focal length. Fine adjustments were made with the aid of a projecting lens positioned at the beam intersection. With this arrangement, interference fringes could be projected on to a screen. The beam splitter was adjusted until the best set of fringes was obtained. After the proper adjustments, the projecting lens was removed. The cell was symmetrically positioned such that the intersecting volume was at the center of the flow channel in a pore space. Its external surfaces were thoroughly cleaned to ensure minimal optical distortion of the laser beams. The measuring point was arbitrarily chosen in the region between the two pressure taps. Subsequent runs were conducted at the same point. The photomultiplier, with a convex collecting lens of 20 cm focal length, was set on an optical bench. For optimal signal strength, it was positioned symmetrically between the two diverging beams. Using the inspection window at the side of the photomultiplier assembly, a focussed image of the beam intersection was obtained. The pin-hole aperture of diameter 0.1 mm was adjusted to fall on the intersecting volume. This step was repeated several times until the best

signal-to-noise ratio was obtained. Plate 2 shows a photograph of the beam intersection (a red X) located in a pore space of cell 2.

With a doppler signal on the oscilloscope, the high voltage supply to the photomultiplier was set to provide an anode current of 5 micro-amps. The amplifier section of the tracker was adjusted to obtain the best signal waveform on the oscilloscope. The doppler frequency could be read off directly from an analogue meter. The value was checked against the frequency estimated from the oscilloscope waveform. This was to ensure that the tracker had locked on to the correct doppler signal. Another output from the frequency tracker was connected to the X-Y recorder to trace the velocity profile. It was driven by its internal time base of 2 sec/inch. The detailed adjustment procedure of the tracker electronics can be found in the manufacturer's handbook for the velocimeter (48).

A needle valve at the inlet to the cell was originally intended for controlling the flow through the system. It was observed that controlling the flow from this point introduced flow perturbations too close to the pressure measuring points. The gate valves of the Rotameters were found to provide better control of the flow.

At each flowrate, the pressure drop across the taps was recorded. The time averaged local velocity was recorded on the X-Y plotter. Runs were repeated to ensure reproducibility. The flow to cell 2 was reversed. In this

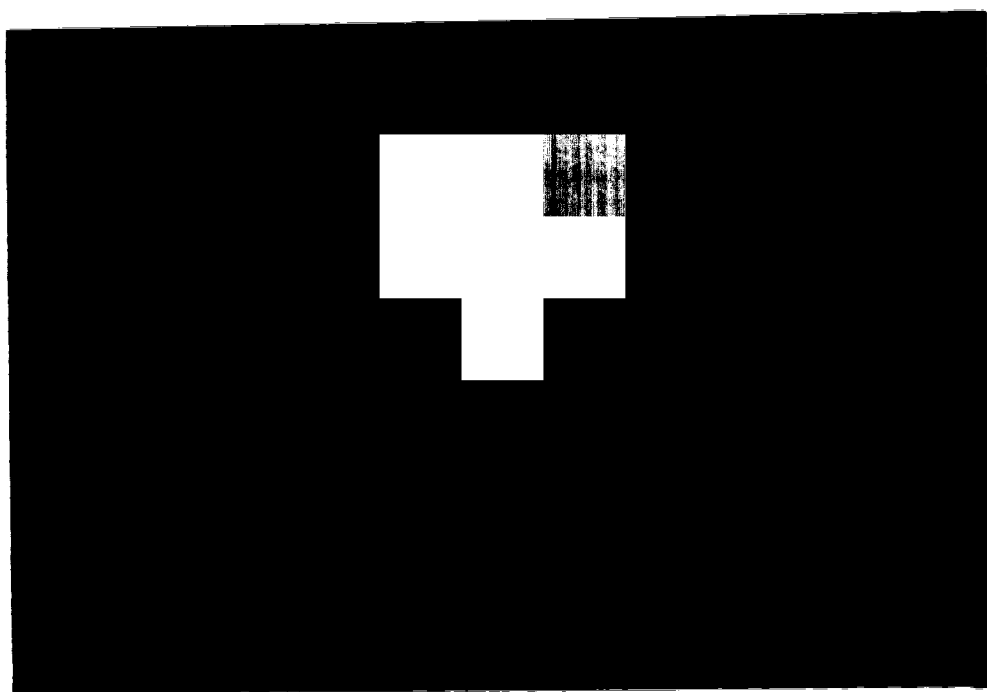


PLATE 2. VIEW OF INTERSECTING BEAMS

case, the cell was referred to as cell 2A. This was undertaken to see if the location of the pressure taps was critical. The pressure transducer of 6.89 kPa rating was used for cell 1. Lower pressure differences were encountered in cells 2 and 2A and the transducer of 0.689 kPa rating was used.

It must be mentioned that the initial alignment was time consuming. However, once completed, it was necessary only to check for the focussed image of the intersecting volume seen through the inspection window of the photomultiplier, and that the pin-hole aperture was positioned over the image before each run.

The beam intersecting angle, θ , used in this study was the largest possible with the Optical Unit. A large angle was necessary to reduce the size of the measuring volume. For a more accurate study of the local velocity, the measuring volume must be as small as possible. This would require a larger intersecting angle to be obtained using some other optical arrangement. The size of the measuring volume in relation to the cross section of the pore space is presented in Appendix 1.

5.4 Treatment of Data

After the data had been processed, a linear least squares fit of the Forchheimer equation was carried out on each set of data to obtain estimates of K and F_b . As the

validity of the Forchheimer equation in the turbulent region has not been established, only data points up to the onset of turbulence were considered.

In spite of the damping effects of the recording pen, the X-Y recorder was used to chart the velocity profiles. It was chosen as it was convenient for recording a continuous profile over a period of time and it presented sufficient qualitative results. For more detailed and quantitative results, the output of the frequency tracker should be fed to some other electronic recording devices such as a magnetic tape recorder.

6. Results

The optical characteristics of the system are presented in Table 4. The calculation of these properties is found in Appendix 1. A large intersection angle was necessary to reduce the size of the measuring volume. However, the size of the angle was limited by the maximum setting of the beam splitter and the clearance between two adjacent spheres in the cell. It can be observed from Equation 16 that a larger angle would give rise to a higher doppler frequency.

No measurements of the porosities of the cells were undertaken. The values indicated in Table 6 were calculated from the physical dimensions of each cell.

The experimental and the processed data are tabulated in Appendix 3 in Tables A.1 through A.6. A sample calculation may be found in Appendix 2. The graphs showing the relationship between the pressure drop, ΔP , and the flowrate, Q , are found in Figures 8 through 10.

Figures 11 through 13 contain the velocity profiles recorded on the X-Y plotter. The vertical axis of each of the traces represents the doppler frequency or indirectly the instantaneous local flow velocity in the pore space. The horizontal axes represent the time base of 2 sec/inch. All the traces have been presented on a scale of 1 : 1.

A steady trace indicates a steady local velocity or streamline flow in the laminar region. At this point, the intermittency factor, γ , is 0. As the flowrate increases, periodic velocity fluctuation is observed (See Figure 11).

Table 4. Properties of Optical Intersection

Beam intersecting angle	21.4°
Width of intersecting volume	0.869 mm
Diameter of intersecting volume	0.164 mm
Fringe spacing	0.0017 mm
No. of interference fringes	96

This is then interpreted as the start of the intermediate zone between the laminar and the turbulent states. Turbulence is reached when the velocity becomes completely unsteady in time and γ is equal to 1. For an accurate determination of the onset of turbulence, a numerical analysis of the instantaneous velocity is necessary. However, a reasonable estimate of the onset of turbulence is summarized in Table 5.

Plate 3 shows the oscilloscope waveforms of some typical bursts of doppler signals. The upper picture shows a burst of doppler signal caused by the presence of a particle in the measuring volume. The lower picture shows another burst of signal as a particle was leaving and another was entering the measuring volume. The arrival of particles in the measuring volume was completely random. Noise was always present in the system and it could be differentiated from the doppler signal by its lower amplitude and irregular periodicity. A reasonable signal strength of 0.5 volt peak-to-peak was obtained.

The pressure gradient versus average velocity relationships are presented in Figures 14 through 16. These graphs also contain the least squares fits of the Forchheimer equation. Table 6 shows the values of k and F_b obtained for each cell from the least squares fit.

The plot of the friction factor, C_f , versus Reynolds number, N_{rp} is displayed in Figure 17. The plot contains data from Cells 1 and 2. It shows the curve as predicted by

Equation 9. The onset of turbulence for each cell has also been indicated. Figure 18 is a similar plot containing only data from Cells 2 and 2A.

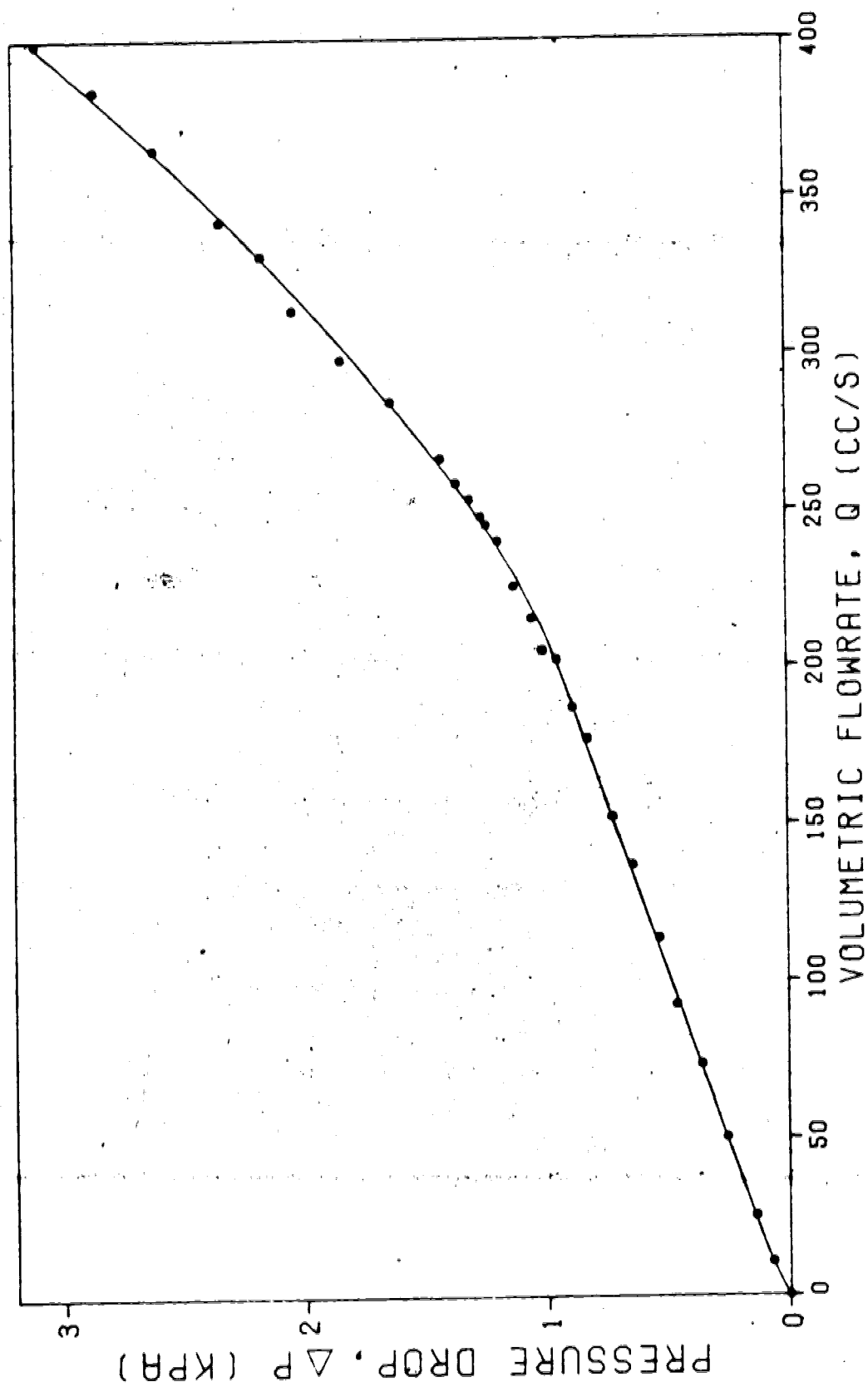


FIG. 8 PRESSURE DROP VS VOLUME FLOWRATE DATA FOR CELL #1

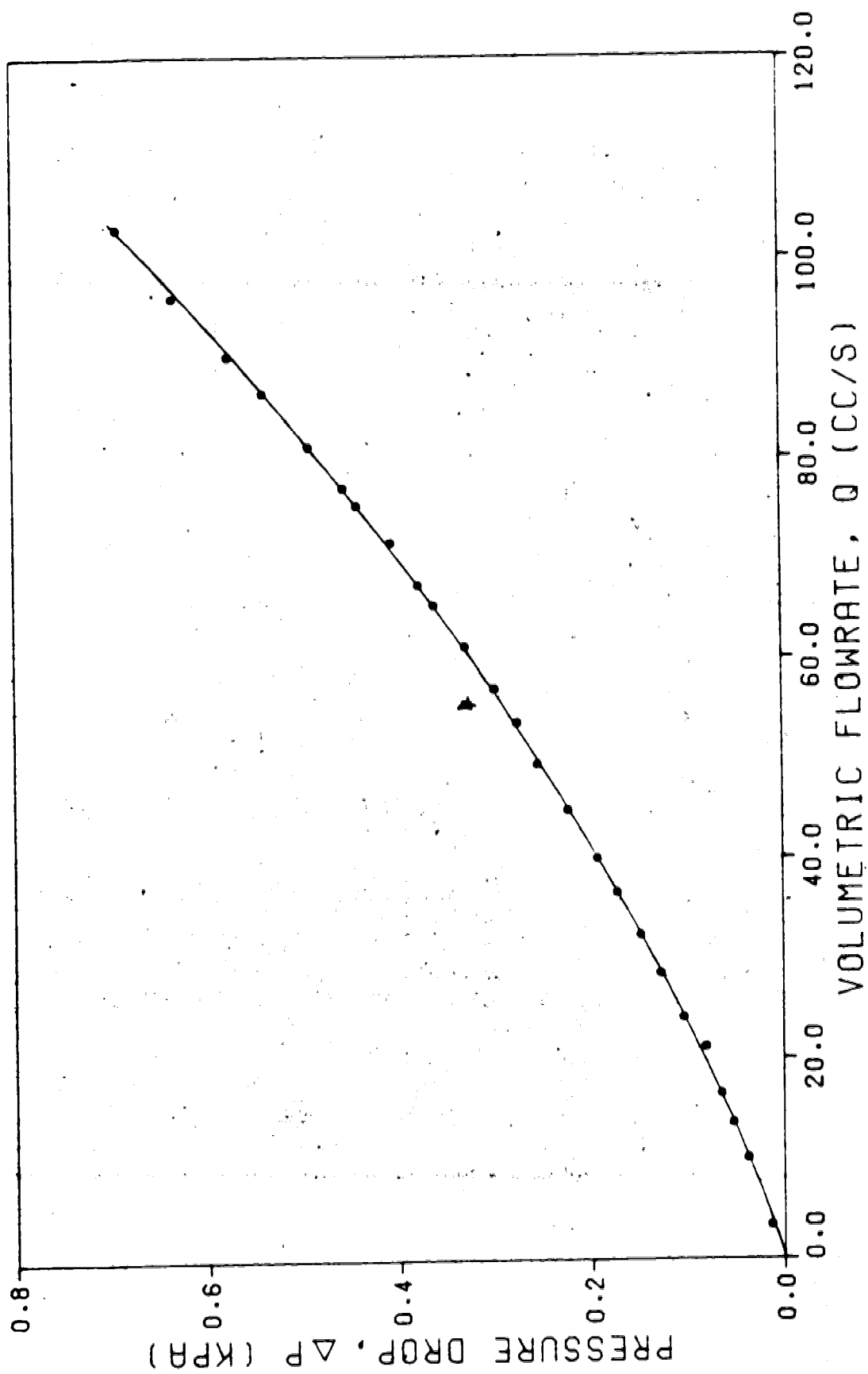


FIG. 9 PRESSURE DROP VS VOLUME FLOWRATE DATA FOR CELL #2

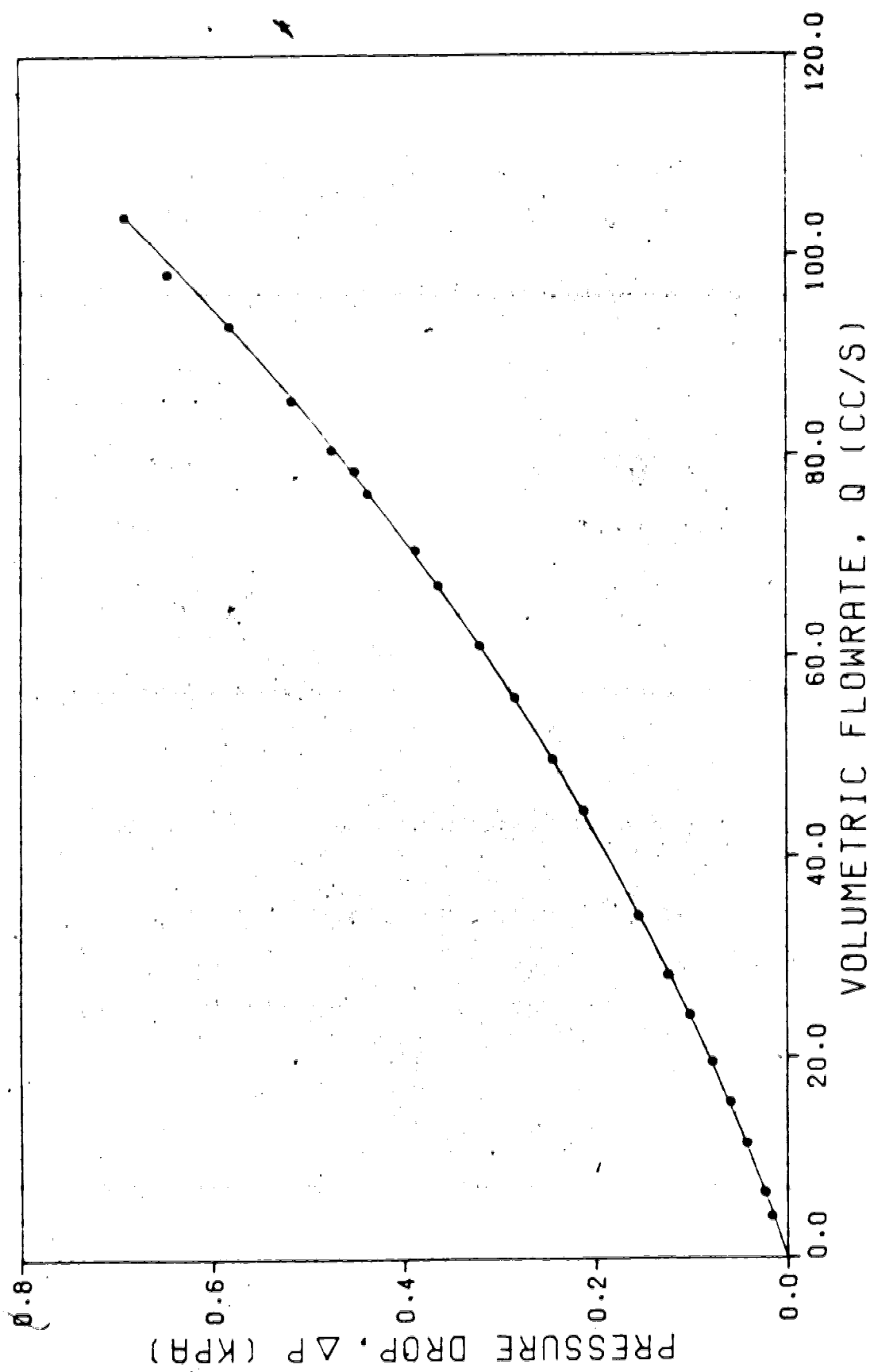


FIG. 10 PRESSURE DROP VS. VOLUME FLOWRATE DATA FOR CELL #2A

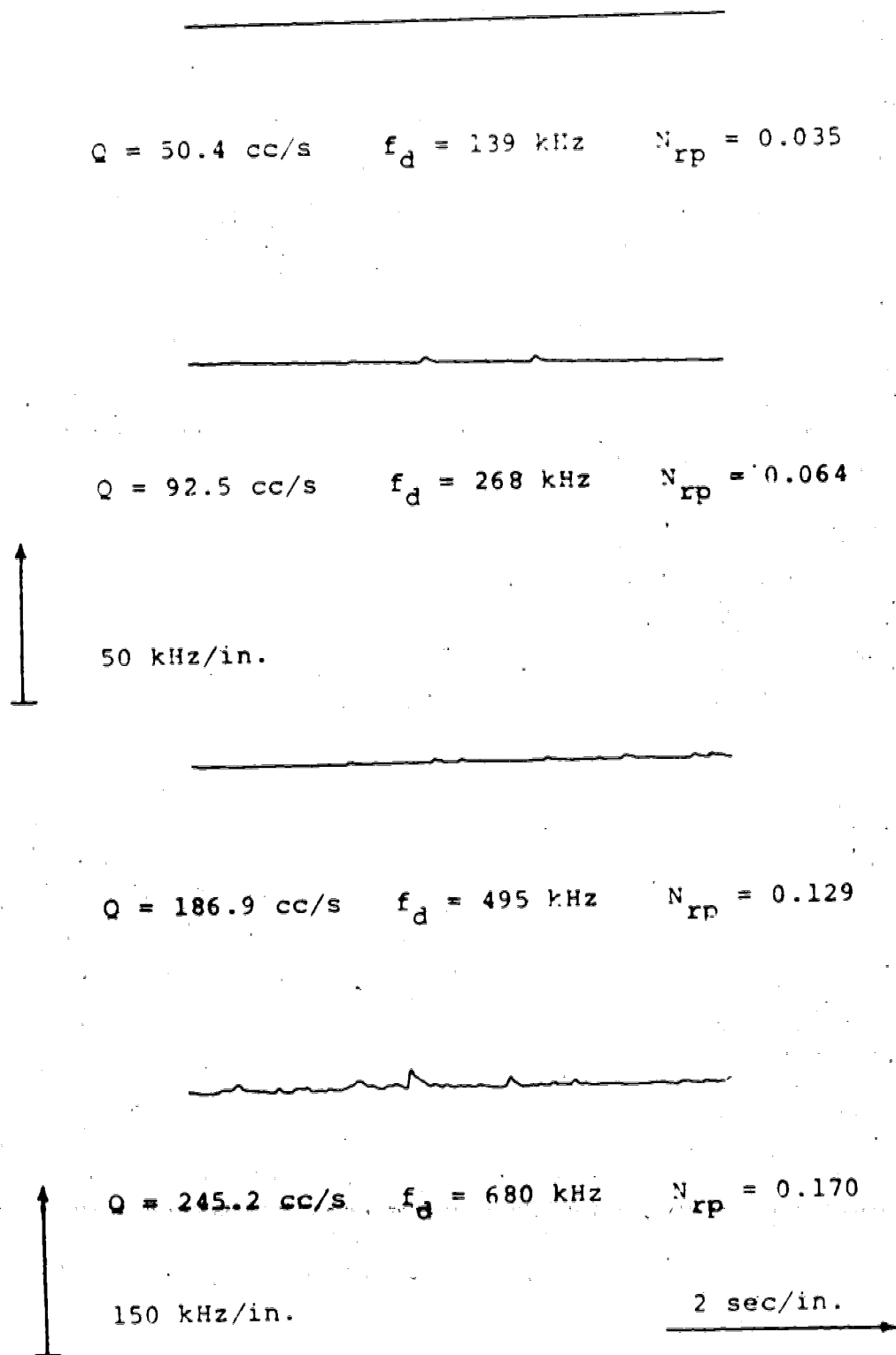

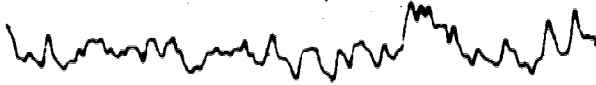



FIG. 11 VELOCITY WAVEFORMS FOR CELL 1




$Q = 258.6 \text{ cc/s}$ $f_d = 720 \text{ kHz}$ $N_{rp} = 0.179$



$Q = 284.6 \text{ cc/s}$ $f_d = 735 \text{ kHz}$ $N_{rp} = 0.197$



$Q = 298.1 \text{ cc/s}$ $f_d = 760 \text{ kHz}$ $N_{rp} = 0.206$



150 kHz/in.

2 sec/in.



FIG. 11 - CONTD.

$Q = 16.47 \text{ cc/s}$ $f_d = 33 \text{ kHz}$ $N_{rp} = 0.135$

$Q = 32.35 \text{ cc/s}$ $f_d = 48 \text{ kHz}$ $N_{rp} = 0.266$


$Q = 65.29 \text{ cc/s}$ $f_d = 49 \text{ kHz}$ $N_{rp} = 0.536$

$Q = 67.29 \text{ cc/s}$ $f_d = 47 \text{ kHz}$ $N_{rp} = 0.553$

15 kHz/in.

2 sec/in.

FIG. 12 VELOCITY WAVEFORMS FOR CELL 2



$Q = 75.29 \text{ cc/s}$ $f_d = 46 \text{ kHz}$ $N_{rp} = 0.618$



$Q = 90.00 \text{ cc/s}$ $f_d = 40 \text{ kHz}$ $N_{rp} = 0.741$



FIG. 12 - CONTD.

$Q = 19.53 \text{ cc/s}$ $f_d = 36.5 \text{ kHz}$ $N_{rp} = 0.163$

$Q = 44.58 \text{ cc/s}$ $f_d = 57 \text{ kHz}$ $N_{rp} = 0.372$


$Q = 61.05 \text{ cc/s}$ $f_d = 54 \text{ kHz}$ $N_{rp} = 0.510$

$Q = 67.05 \text{ cc/s}$ $f_d = 53.5 \text{ kHz}$ $N_{rp} = 0.560$

15 kHz/in.

2 sec/in.

FIG. 13 • VELOCITY WAVEFORMS FOR CELL 2A




$Q = 76.23 \text{ cc/s}$ $f_d = 52.5 \text{ kHz}$ $N_{rp} = 0.637$



$Q = 93.0 \text{ cc/s}$ $f_d = 56 \text{ kHz}$ $N_{rp} = 0.777$

15 kHz/in.



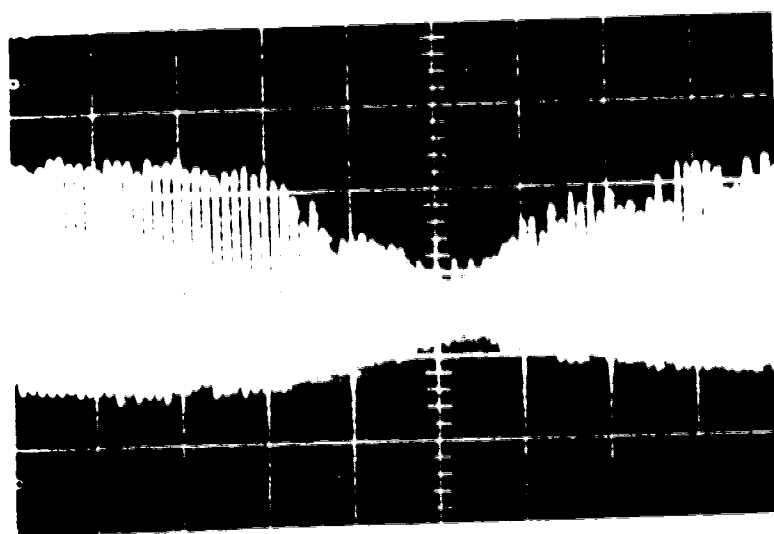
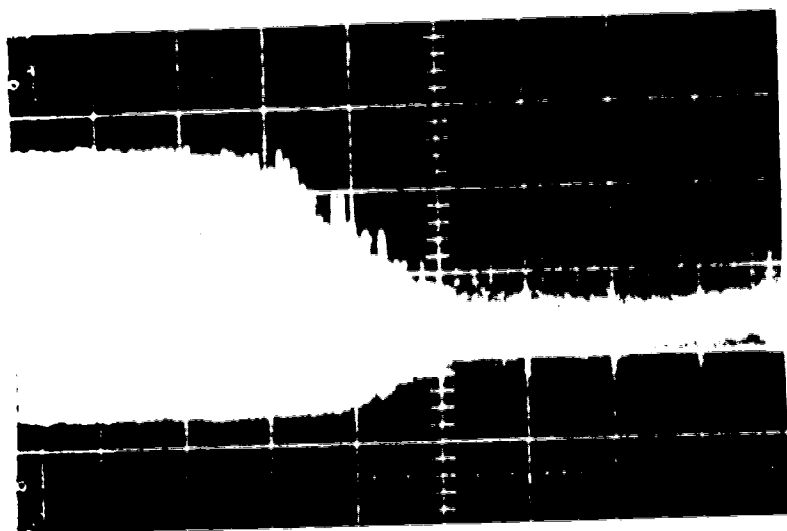
2 sec/in.



FIG. 13 - CONTD.

Table 5. Critical Values at Onset of Turbulence

Cell #	Q (cc/s)	f_d kHz	N_r	N_{rp}
1	258.6	720	104	0.179
2	• 75.29	45.5	41.7	0.618
2A	76.23	52.5	42.2	0.627



Y axis: 0.2 volt/cm X axis : 0.2 ms/cm

Cell 1: $Q = 18.0$ cc/s $f = 42.5$ KHz

PLATE 3. OSCILLOSCOPE WAVEFORMS OF DOPPLER SIGNALS

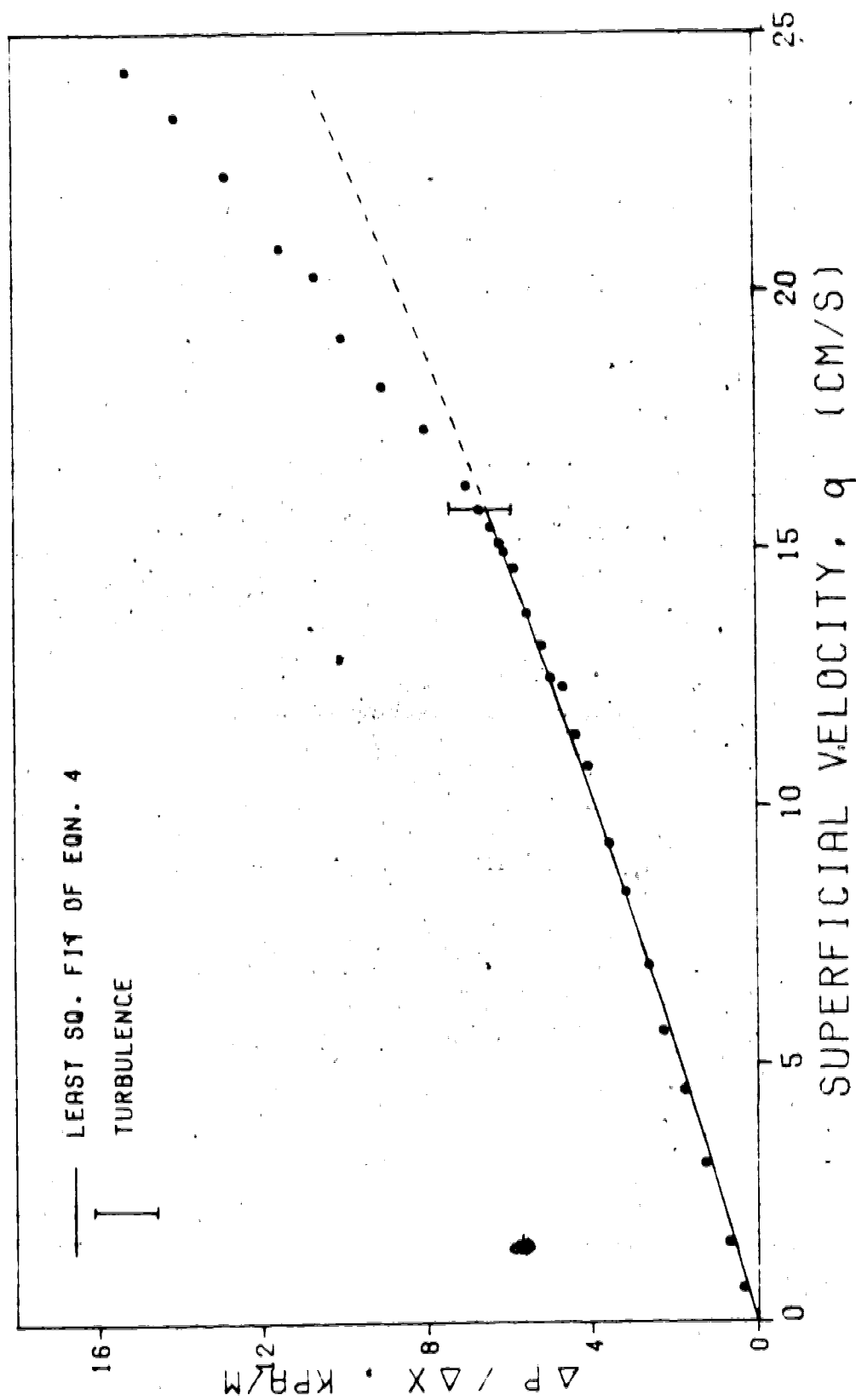


FIG. 14 PRESSURE GRADIENT VS SUPERFICIAL VELOCITY - CELL #1

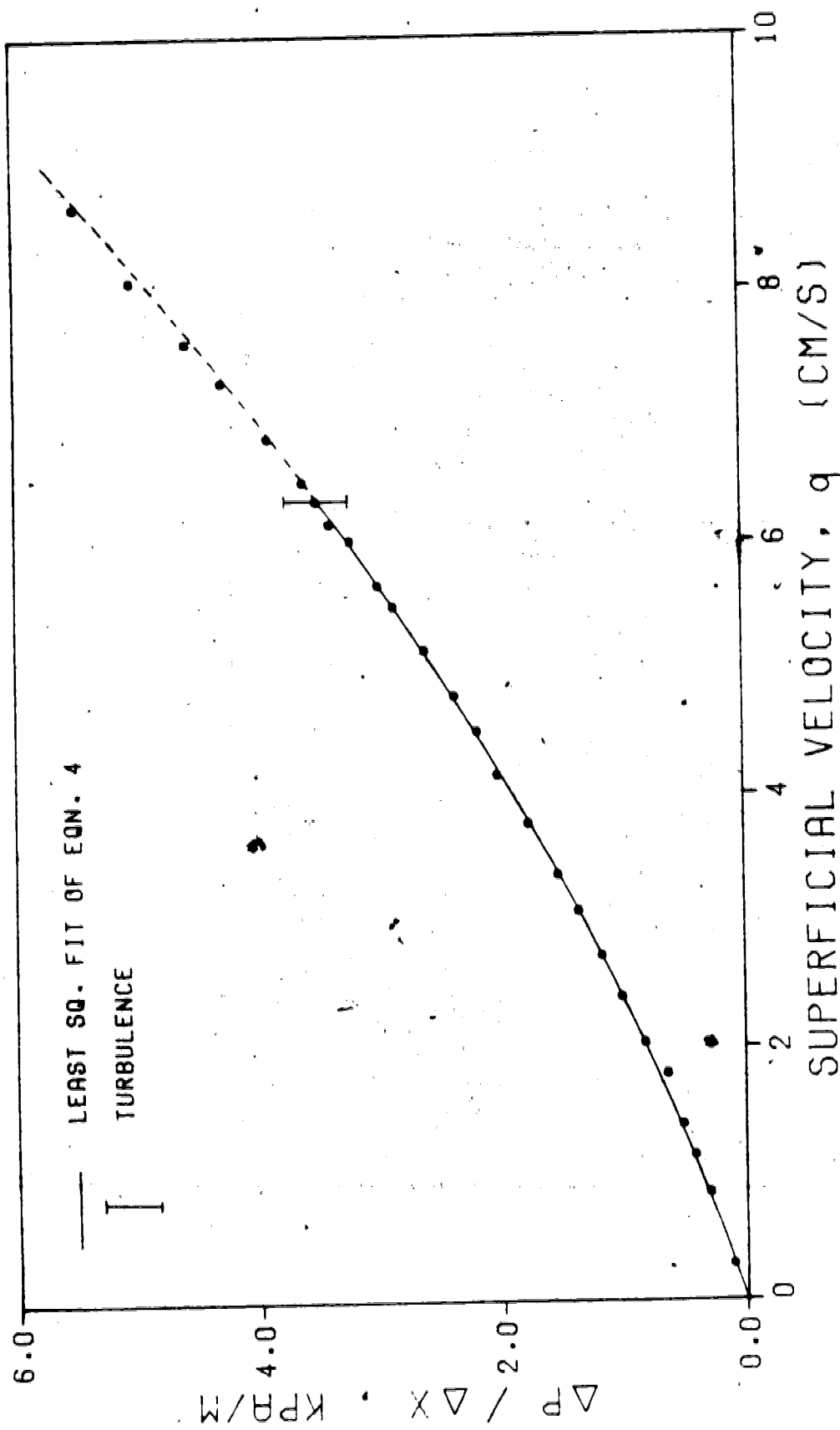


FIG. 15 PRESSURE GRADIENT VS SUPERFICIAL VELOCITY - CELL #2

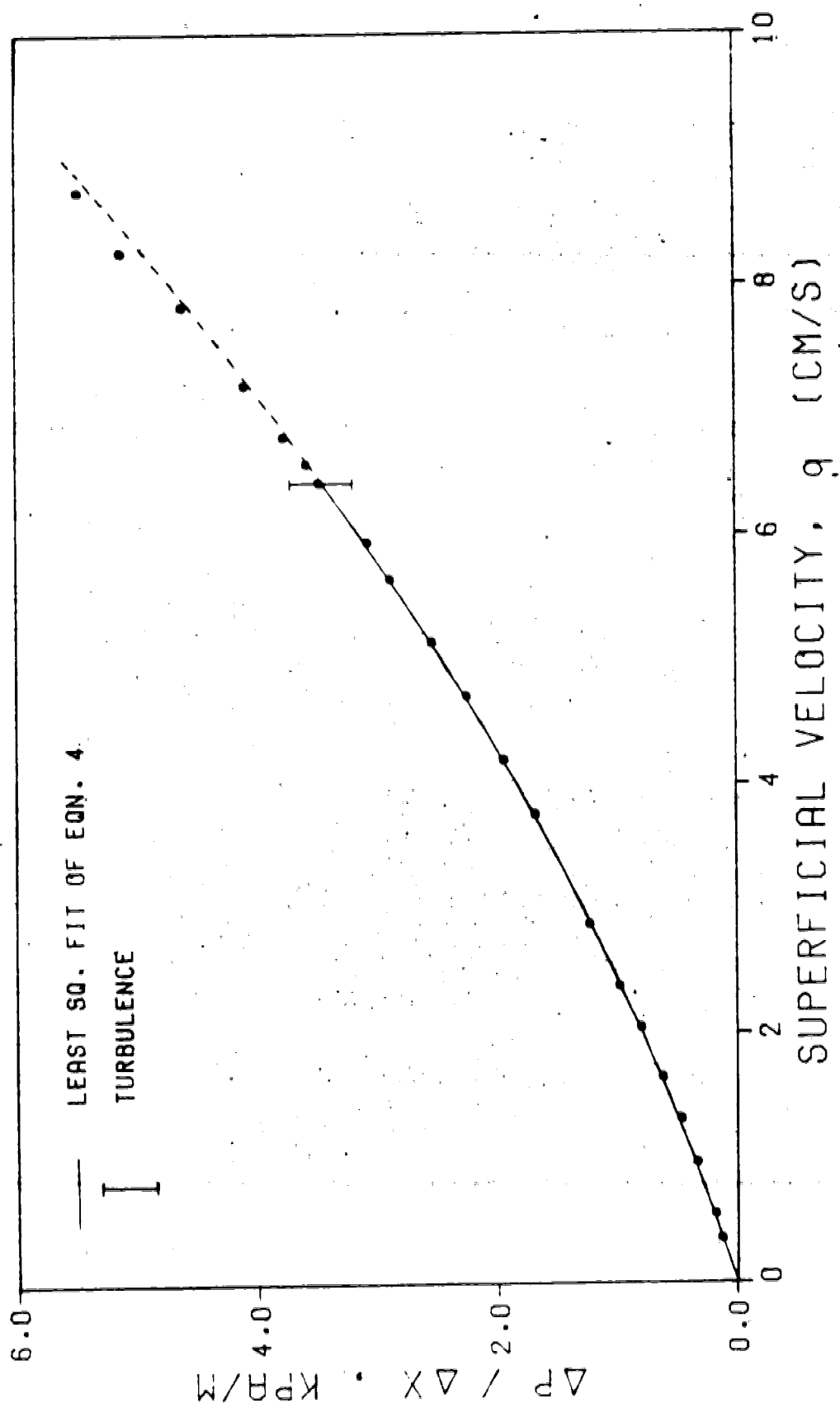


FIG. 16 PRESSURE GRADIENT VS SUPERFICIAL VELOCITY - CELL #2A

Table 6. Characteristics of Porous Media

Cell #	Porosity %	K ($\times 10^{-7}$) m^2	F _b 1/m
1	47.64	4.7395	48.60
2	47.64	4.8313	389.5
2A°	47.64	4.9967	383.0

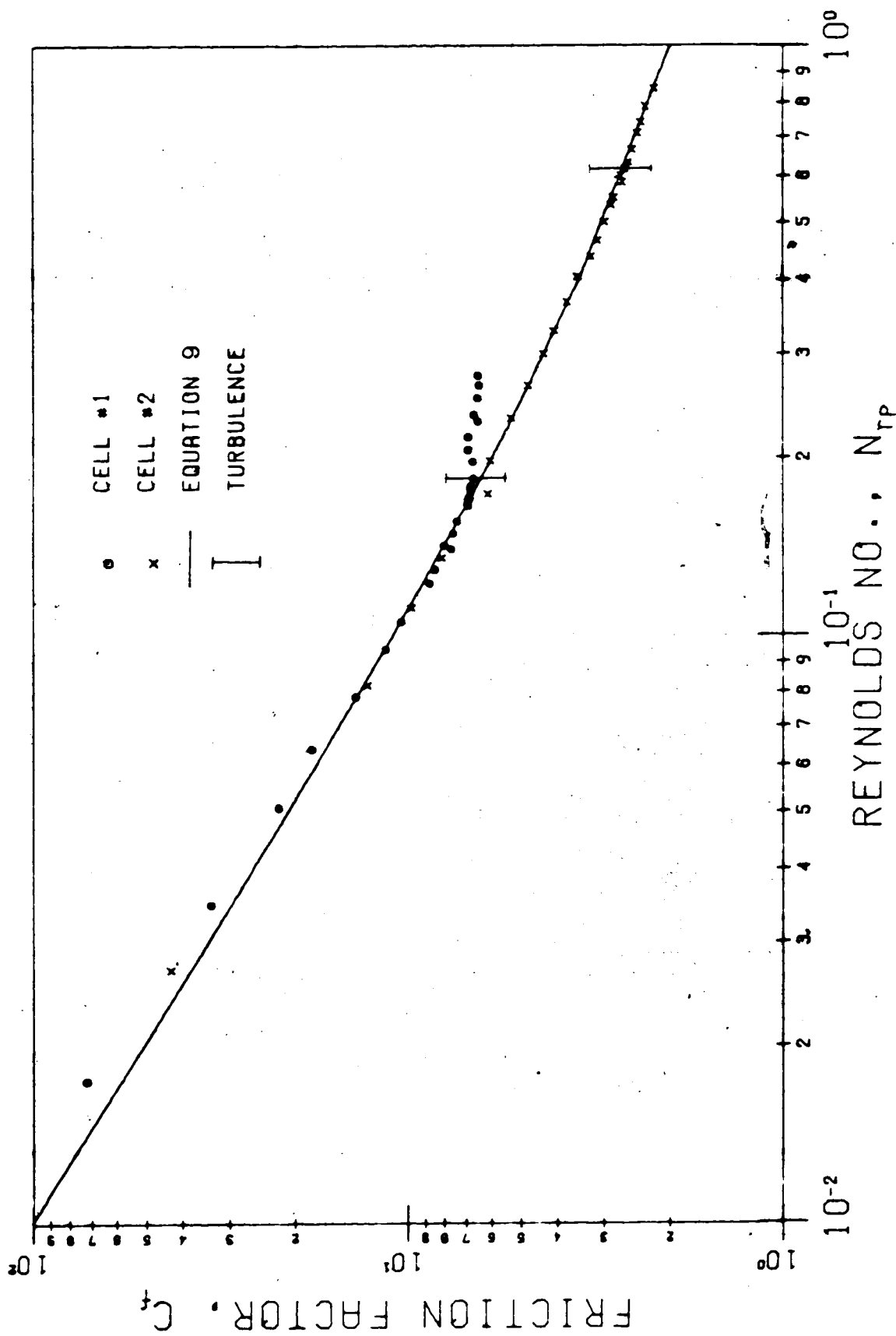


FIG. 17 PLOT OF FRICTION FACTOR VS REYNOLDS NO.

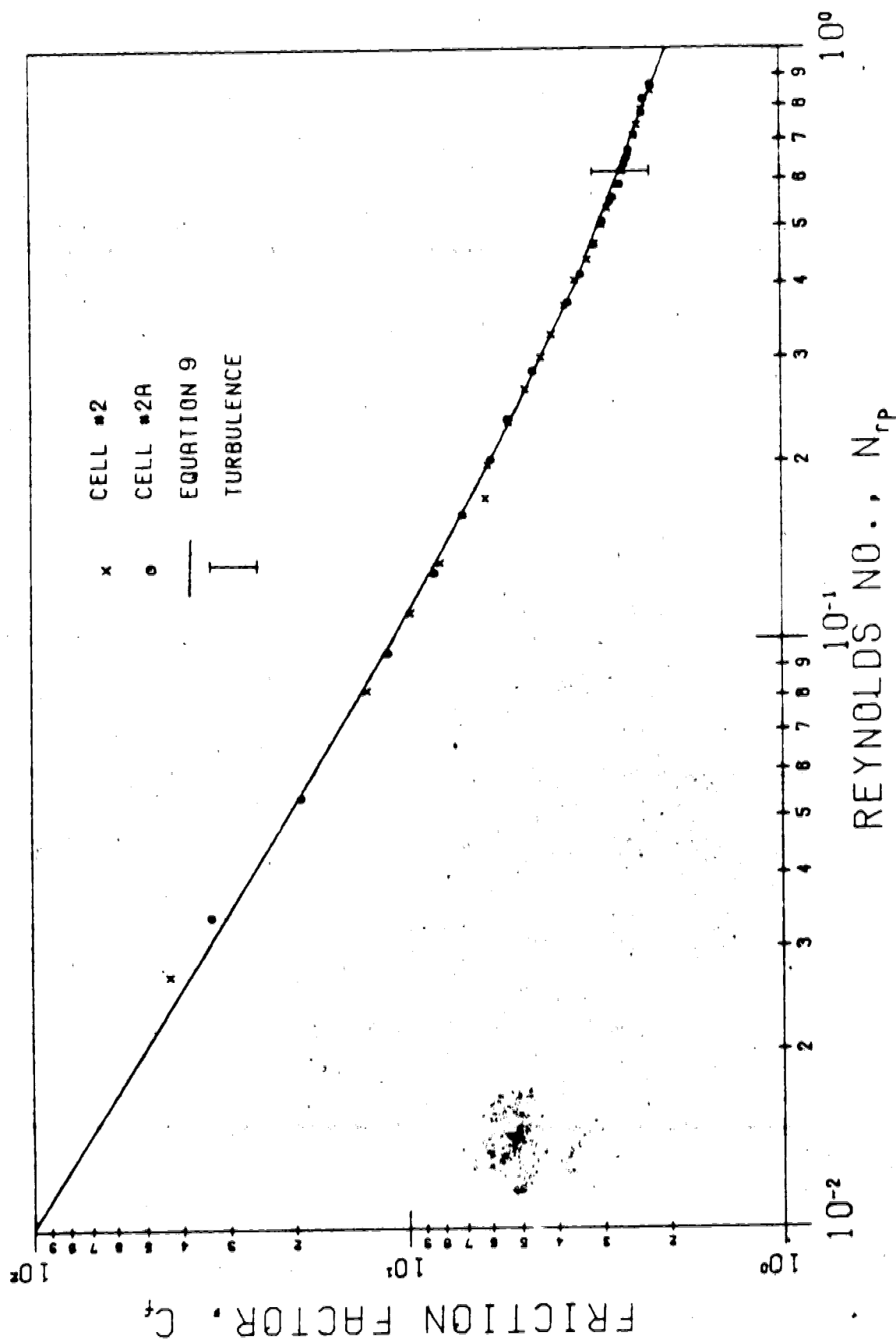


FIG. 18 PLOT OF FRICTION FACTOR VS REYNOLDS NO. - CELL 2

7. Discussion

A small scatter of data is observed in both cells with less appearing in Cell 2. In the case of Cell 2, values of ΔP were recorded. This was due to the shorter distance between the pressure taps in Cell 2. Pressure differences less than 0.19 kPa have been extrapolated from the calibration of pressure transducer 2.

The data of Cell 1 were recorded with the intersecting volume positioned symmetrically in the pore space. Runs were repeated with the intersecting volume placed as close as possible to the smallest regions of the pore space. Random velocity fluctuations were observed at lower flowrates than with the intersecting volume at the widest section of the pore space. However, McFarland (49) reported uniform occurrence of turbulence in the pore space. The birefringence technique is a qualitative method and its visual quality depends on the magnification of the optical system. It is possible that the velocity fluctuation in the smaller sections of the pore space could not be observed with the visual resolution he had in his study.

Flow through the narrower sections of the pore is faster and can give rise to wakes and vortices. The velocity fluctuations in these sections recorded by the velocimeter may have been due to these flow phenomena.

In Cell 2, turbulence occurred almost at the same superficial velocity in most parts of the pore space. The data reported were those with the measuring volume placed in

the middle of the pore space.

An inspection of the cross section of Cell 1 (see Figure 5) which has a converging and diverging cross section suggests that the flow would be mainly rectilinear. On the other hand, curvilinear flow would be more likely to occur in Cell 2. This was verified when streams of air bubbles were occasionally observed to travel downstream in the cells. This observation is interesting and does help to explain the following results.

Figure 14 shows that with Cell 1, the Forchheimer equation fitted with data points up to the onset of turbulence could not be used to predict the pressure drop in the turbulent region. On the other hand with Cell 2, Figures 15 and 16 indicate that the Forchheimer equation provides reasonable prediction of the pressure drop even for flow well into turbulence.

Another interesting observation is illustrated in Figure 17 which shows a plot of the friction factor, C_f , versus Reynolds number, N_{rp} . It has been discussed earlier in a previous section that the use of the N_{rp} is preferred over N_r for the definition of the Reynolds number. As such, only plots of C_f versus N_{rp} will be shown. Such plots demonstrate the agreement between the experimental data and the theory defining C_f and N_{rp} .

After the onset of turbulence in Cell 1, there is a departure of the data points from the theoretical curve predicted by Equation 9. This resembles a similar

correlation in the case of a straight pipe. There is good agreement between the data and the theory in the case of Cell 2. Unfortunately, a comparison of the same plot for Cell 1 by McFarland (50) cannot be made as he could not record any observation of turbulence with the glycerine solution due to the small pressure head available (51).

The results shown in Figure 17 suggest that it may be inaccurate to characterize a porous medium as a series of straight flow channels with converging and diverging cross sections. Houpert (52) considered a porous medium to have a cross section similar to that of cell 1 in his derivation of the quadratic form of the pressure gradient and superficial velocity relationship. Though his equation may have the form of the Forchheimer equation, his approximation of the porous medium is questionable since the flow would be mainly rectilinear. Houpert (53) and Katz et al. (54) attribute the extra pressure loss in non-Darcy flow to the inertial effects of the fluid flowing through constricting passages. Though this may be partly the case, it is reasonable to assume that curvilinear flow makes a greater contribution to the extra pressure drop. Jones (55) interprets the departure from Darcy flow as being caused by secondary flow due to the curvature of the pores. Such flows have been observed in early experiments with curved pipes by White (56) and Taylor (57).

The velocity traces, Figures 11 through 13, indicate that the intermediate region in Cell 1 extends over a wider

range of flowrate. This intermediate region is characterized by increasing periods of 'spiky' velocity fluctuations. These observations are similar to those referred to by Schlichting (58) in his discussion of the transition zone in a straight pipe. No clearly defined intermediate zone was observed with Cell 2. A higher magnitude of the fluctuation, u , was observed in Cell 1 than in Cell 2. This indicates that there was higher intensity of turbulence in Cell 1.

The effect of flow geometry is also evident in the results of Table 4. In particular, Cell 2 has a much higher inertial resistance coefficient F_b , although both cells have the same value of porosity. This suggests that F_b is dependent on path curvature. It can be observed from the processed data in Appendix 3 that for a particular superficial flow rate, a higher pressure gradient occurred in Cell 2 than in Cell 1. The higher values of F_b and pressure gradient suggest that the flow in Cell 2 was more curvilinear than in Cell 1. Table 7 compares the results of Cell 1 with those obtained by McFarland (59). There is a one and a half times difference between the estimates of F_b obtained from the two studies. The repack of the cell could have contributed to the difference. The more probable cause may be the fact that there were insufficient data points in McFarland's estimation of F_b from the data using the glycerine solution.

Table 8 contains a comparison of the Reynolds number, N_r , at the onset of turbulence with those of some authors in the

literature. The values of N_r from this work are 104 and 41.9 (an average of the values for Cells 2 and 2A). It is observed that the results of Cell 2 show better agreement with those of Schneebeli (60) and Kyle and Perrine (61). Both groups of researchers conducted experiments in which the flows were mainly curvilinear.

The results obtained here support the view that it is reasonable to use KF_b as the length parameter in the definition of Reynolds number although no single value of Reynolds number could be found to describe the onset of turbulence. The use of the C_f vs N_{rp} correlation helps to illustrate the type of flow occurring in the medium.

No attempt has been made to mathematically describe turbulent flow in porous media due to the time constraints on this study. However, this research has established the preliminary work for further studies using the laser doppler velocimeter. It has also helped to indicate what some of the desirable features of future research should be. Eventually more random packs of different sphere diameter should be used. An attempt was made to view the intersecting volume through the lucite spheres. Results indicated that measurements may be obtained with the existing velocimeter and a random pack. There were, however, refraction and attenuation of the laser beams. The difference between the refractive indices of the lucite and the oil was responsible for these effects. This would suggest that the refractive indices should be matched and a laser unit of higher output

be used. The resulting lower signal-to-noise ratio in a random pack may require the use of better tracking capabilities of the signal processor. An example of such a processor is the Disa Type 55N20 Doppler Frequency Tracker (62).

Table 7. Comparison of Results from Cell #1

Reference	K ($\times 10^{-7} \text{ m}^2$)	F (1/m)	N_{rp}	N_r
McFarland	3.5164	70.73	0.241	123
This work	4.7395	48.60	0.179	104

The Reynolds numbers quoted refer to the values at the onset of turbulence ($\gamma = 1$).

Table 8. Comparison of N_r with those in literature

Author	Pack Description	N_r
Schneebeli	27 mm spheres & 1 in. gravel - random	60
Wegner, Karabelas & Hanratty	3 in. sphere - cubic	90 - 120
Kyle & Perrine	2-D arrays of 1.5 in. cylinders	55 - 137
Kingston & Nunge	1.5 in. spheres	80
McFarland	0.5 & 0.25 in. cubic packs	128 - 251
This work	0.5 in. cubic pack #1 pack #2 pack #2A	104 41.7 42.2

8. Conclusions

This study has successfully demonstrated the use of the laser doppler velocimeter for flow measurements in a porous medium over a range of flowrates. As a result, the following conclusions can be made.

1. A porous medium should not be represented by a series of straight flow channels of converging and diverging cross sections as flow through such channels is mainly rectilinear and approximates that through straight pipes. The flow geometry should include the curvilinear path of the fluid.
2. The region between the Darcy and the turbulent regimes may be described as a zone of increasing fluctuation in the flow. The extent of this intermediate zone depends on the flow geometry. Flow which is mainly curvilinear gives rise to an intermediate zone much shorter than that arising from rectilinear flow.
3. The Forchheimer equation may have to be modified if it is to be used to predict the pressure drop in the turbulent region.
4. The choice of the length parameter in the definition of the Reynolds number is yet to be established. However the Reynolds number as defined by N_{rp} suggests that KF_b is a reasonable choice as N_{rp} has been shown to have a

mechanistic base.

5. The laser doppler velocimeter is an excellent instrument for non-intrusive flow studies. It can be used for quantitative and qualitative studies of the characteristics of flow regimes and in particular the transition to turbulence.

6. With effective flow diffusers, the location of the pressure taps in the cell is not critical.

9. Recommendations

The effort to describe turbulent flow in a porous medium is a continuous process. To this end, the following recommendations are made.

1. With the present velocimeter, further flow studies should be performed using cells with packing arrangements which would eliminate rectilinear flow. This would serve to indicate how the onset of turbulence is affected by the curvature of the flow.
2. Further experiments with cell 2 should be conducted by increasing the flowrate well beyond those encountered in this study. This is to verify that the onset of turbulence indicated in this study is indeed so. The cell has not been tested to see if it could withstand the higher pressure associated with higher flowrates. This is an important factor when considering future designs of cells which are to accommodate turbulent flows.
3. A random packing of smaller diameter spheres should eventually be used to simulate the porous medium. This would require the use of a more powerful laser unit. The refractive indices of the lucite spheres and the oil should be matched. The laser beams will then travel through the oil and the spheres with minimal refraction. Attenuation in the light intensity would give rise to a lower signal-to-noise

ratio. It may then be necessary to switch to a form of signal analysis other than frequency tracking as used in this study.

4. As there is a limit to the gravity-fed pressure head available, it may be worthwhile to investigate if an input pump could be used without introducing perturbation to the flow. In this case, care must be taken to isolate the laser velocimetry equipment from the machine vibration.

5. The needle valve for controlling the flow should be placed as far upstream as possible from the inlet to the cell to reduce flow perturbation which results in fluctuating pressure changes.

Nomenclature

A	= cell cross-sectional area, cm^2
a	= constant in Forchheimer equation
b	= constant in Forchheimer equation
C_f	= friction factor, dimensionless
c	= constant in Equation 3
D	= average particle or sphere diameter, m
D_e	= beam diameter at $1/e^2$ intensity, m
d	= diameter of intersecting volume, m
\hat{e}_i	= unit vector of incident beam
\hat{e}_s	= unit vector of scattered beam
F_a	= viscous resistance coefficient, m^{-2}
F_b	= inertial resistance coefficient, m^{-1}
f	= focal length of lens, m
f_a	= doppler frequency, Hz
f_i	= incident beam frequency, Hz
f_m	= frequency of measured signal, Hz
f_s	= scattered beam frequency, Hz
k	= permeability, m^2
M	= fluid mass flowrate, g/s
m	= constant in Equation 3
N_f	= number of fringes in measuring volume
N_r	= Reynolds No. based on sphere diameter
N_{rp}	= Reynolds No. defined for porous medium
Q	= volumetric flowrate, cm^3/s
q	= superficial velocity, cm/s

U	= local velocity, m/s
U_m	= time averaged local velocity, m/s
u	= fluctuation of local velocity, m/s
w	= width of intersecting volume, m
x	= horizontal distance along cell, m
ΔP	= pressure drop across taps, Pa/m
Δs	= fringe spacing, m
Δt	= transit time of particle crossing fringes, s
Δx	= distance between pressure taps, m
n	= refractive index of medium
n_l	= refractive index of liquid
θ	= beam intersecting angle, deg
θ_l	= beam intersecting angle in liquid, deg
λ	= laser wavelength, m
λ_l	= laser wavelength in liquid, m
μ	= fluid viscosity, Pa.s
ρ	= fluid density, kg/m ³

References

1. McFarland, J.D., 'Transition to Turbulence in Porous Media', M.Sc. Thesis, Department of Mineral Engineering, University of Alberta, 1975.
2. Irmay, S., 'On the Theoretical Derivation of Darcy and Forchheimer Formulas', Trans. Amer. Geophy. Union, 39 pg. 702, 1958.
3. Hubbert, M King, 'The Theory of Ground-water Motion', Journal of Geology, 48 p. 8, 1940.
4. Schneebeli, G., 'Experiments on the Range of Validity of Darcy's Law and the Appearance of Turbulence in a Filtering Flow', La Houille Blanche, No. 2, p. 141, 1955.
5. Chauvateau, G. and Thirriot, Cl., 'Regimes d'Ecoulement en Milieu Poreux et Limite de la Loi de Darcy', La Houille Blanche, No. 2, p. 141, 1967.
6. Wright, D.E., 'Nonlinear Flow Through Granular Media', Journal of Hydraulics Div., Proceedings ASCE, 94, HY 4, p. 851, 1968.
7. Kingston, G. and Nunge, R., 'Transition to Unsteady Flow and Intensity of Velocity Fluctuations in a Porous Medium', Can. J. Ch. Eng. 51, p. 245, 1973.
8. McFarland, J.D. and Dranchuk, P.M., 'Visualization of the Transition to Turbulent Flow in Porous Media', J. Can. Pet. Tech., 15, No. 2, p. 71, 1976.
9. Forchheimer, P., 'Wasserbewegung durch Boden', Z. der. deut. Ing., 45, p. 1782, 1901.
10. Scheidegger, A.E., 'The Physics of Flow Through Porous Media', University of Toronto Press, p. 127, 1974.
11. Trollope, D.H., Stark, K.P. and Volker, R.E., 'Complex Flow Through Porous Media', Australian Geomech. J., G1, No. 1, pp. 1-10, 1971.

12. Irmay, S., op. cit., p. 705
13. Chywi, E., 'An Analysis of Transient Gas Flow Through Porous Media', M.Sc. Thesis, Department of Chemical and Petroleum Engineering, University of Alberta, pp. A2-A16, 1968.
14. Green, L. Jr., and Duwez, P., 'Fluid Flow Through Porous Metals', Trans. ASME, J. App. Mech., 79, p. 39, 1951.
15. Chalmers J., Taliaferro Jr., D.B., and Rawlins, E.L., 'Flow of Air and Gas Through Porous Media', Trans. AIME, 98, p. 375, 1932.
16. Fancher, G.H. and Lewis, J.A., 'Flow of Simple Fluids Through Porous Materials', Ind. Eng. Chem., 25, No. 10, p. 1139, 1933.
17. Green, L. Jr. and Duwez, P., op. cit., p. 39
18. Green, L. Jr. and Duwez, P., loc. cit.
19. Schneebeli, G., op. cit., p. 143
20. Chauvateau, G. and Thirriot, Cl., op. cit., p. 141
21. Wegner, T.H., Karabelas, A.J. and Hannratty, T.J., 'Visual Studies of Flow in a Regular Array of Spheres', Chem. Eng. Sci., 26, p. 59, 1971.
22. Kyle, C.R. and Perrine, R.L., 'An Experimental Model for Visual Studies of Turbulent Flow in Porous Material', Can. J. Chem. Eng., 49, p. 19, 1971.
23. McFarland, J.D., op. cit., p. 8
24. Wright, D., op. cit., p. 853
25. Kingston, G and Nunge, R.J., op. cit., p. 246

26. van der Merwe, D.F. and Gauvin, W.H., 'Velocity and Turbulence Measurements of Air Flow Through a Packed Bed', AICHE J., 17, p. 519, 1971.
27. Yeh, Y. and Cummins, H.Z., 'Localized Fluid Flow Measurements with a He-Ne Laser Spectrometer', Appl. Phys. Letters, 4, p. 176, 1964.
28. Foreman Jr., J.W., Lewis, R.D., Thornton, J.R. and Watson, H.J., 'Laser-Doppler Velocimeter for Measurement of Localized flow Velocities in Liquids', Proc. IEEE, 54, p. 70, 1966.
29. Goldstein, R.J. and Kreid, D.K., 'Measurement of Laminar Flow Development in a Square Duct Using a Laser-Doppler Flowmeter', Trans. ASME, J. Appl. Mech., 89, p. 813, 1967.
30. Berman, N.S. and Santos, V.A., 'Laminar Velocity Profiles in Developing Flows Using a Laser-Doppler Technique', AICHE J., 15, p. 323, May 1969.
31. Goldstein, R.J. and Kreid, D.K., loc. cit.
32. Goldstein, R.J. and Hagan, W.F., 'Turbulent Flow Measurements Utilizing the Doppler Shift of Scattered Laser Radiation', Phys. of Fluids, 10, p. 1349, 1967.
33. Humphrey, R.L., 'Using Lasers for Flow Measurement', Instr. Contr. Syst., p. 75, Nov. 1972.
34. Durrani, T.S. and Greated, C.A., 'Laser Systems in Flow Measurement', Plenum Press, N.Y. 1977.
35. Johnston, W., Dybbs, A. and Edwards, R., 'Laser Anemometer Measurement of Fluid Velocity in Porous Media', Proc. of the Second International Workshop on Laser Velocimetry, 2, p. 433, Purdue University, 1974.
36. Watrasiewicz, B.M. and Rudd, M.J., 'Laser Doppler Measurement', Butterworths, England, p. 22, 1976.

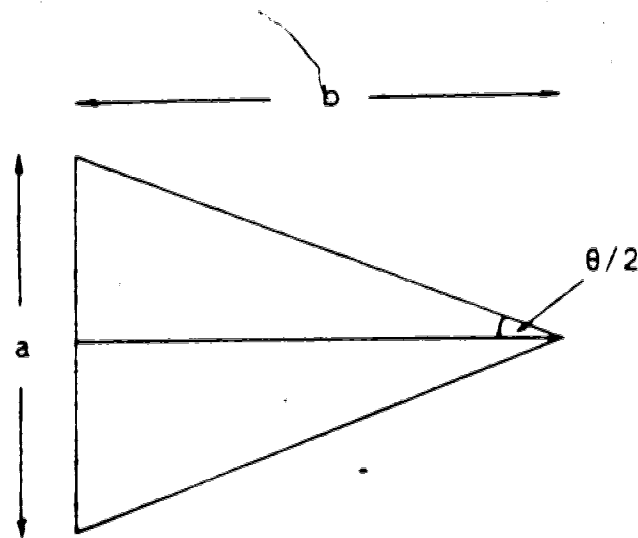
37. Schlichting, H., 'Boundary Layer Theory', McGraw Hill, USA, p. 377, 1960.
38. Durst, F., Melling, A. and Whitelaw, J. H., 'Principles and Practice of Laser Anemometry', Academic Press, New York, p. 97, 1976.
39. Watrasiewicz, B.M. and Rudd, M.J., op. cit., p. 37
40. Rudd, M.J., 'A new theoretical model for the laser Dopplermeter', J. Sci. Instr., 2, Series 2, 55, 1969.
41. Longhurst, R.S., 'Geometrical and Physical Optics', Longmans, London, 1967.
42. Longhurst, R.S., op. cit., p. 466
43. Vlachos, N.S., Whitelaw, J.H., 'The Measurement of Blood Velocity with Laser Anemometry', Proc. of Second International Workshop on Laser Velocimetry, 1974, Purdue University, p. 521
44. Parker, J.D., Boggs, J.H. and Blick, E.F., 'Introduction to Fluid Mechanics and Heat Transfer', Addison Wesley Publ. Co., p. 61, 1969.
45. Schlichting, H., op. cit., p. 378
46. McFarland, J.D., op. cit., p. 17
47. Goldstein, R.J. and Kreid, D.K., op. cit., p. 815
48. Disa Electronics Ltd., 'Type 55L Laser Doppler Anemometer - Instructional Manual', Denmark, 1973.
49. McFarland, J.D., op. cit., p. 50
50. McFarland, J.D., op. cit., p. 44

51. Dranchuk, P.M., University of Alberta, private communication.
52. Houpert, A., 'On the Flow of Gases Through Porous Media', Revue de L'Institut Francais Du Petrole, 14, p. 1477, 1959.
53. Houpert, A., loc cit.
54. Katz, D.L. et al., 'Handbook of Natural Gas Engineering', McGraw Hill Book Co., New York, p. 47, 1959.
55. Jones, W.M., 'Viscous Drag and Secondary Flow in Granular Beds', Brit. J. Appl. Phys., Ser. 2, 1, 1559, 1968.
56. White, C.M., 'Streamline Flow Through Curved Pipes', Proc. Roy. Soc. (London), Ser. A, 123, p. 645, 1929.
57. Taylor, G.I., 'The Criterion of Turbulence in Curved Pipes', Proc. Roy. Soc. (London), Ser. A, 124, p. 243, 1929.
58. Schlichting, H., op. cit., p. 377
59. McFarland, J.D., op. cit., p. 33
60. Schneebeli, G., loc. cit.
61. Kne, C.R. and Perrine, R.L., loc. cit.
62. 'Laser Doppler Anemometry Equipment Catalog', Disa Electronics, Denmark 1978.

Appendix 1.

Calculation of Properties of Optical Intersection

- a) Using the geometry formed by the two intersecting laser beams, the angle $\theta/2$ is calculated from the equation given below.



$$\theta/2 = \tan^{-1} \left(\frac{a/2}{b} \right)$$

$$a = 3.85 \text{ cm}$$

$$b = 10.20 \text{ cm}$$

$$\begin{aligned} \therefore \theta/2 &= \tan^{-1} \left(\frac{3.85}{2 \times 10.20} \right) \\ &= 10.7^\circ \end{aligned}$$

b) Intersecting Volume

Given

$$\theta/2 = 10.7^\circ$$

$$\lambda = 6328 \times 10^{-10} \text{ m}$$

$$D_e = 0.65 \times 10^{-3} \text{ m}$$

$$f = 0.13 \text{ m}$$

i) Using Equation 22,

$$\begin{aligned} w &= \frac{4}{\pi} \cdot \frac{(\lambda)(f)}{D_e} \cdot \frac{1}{\sin(\theta/2)} \\ &= \frac{4}{\pi} \cdot \frac{(6328 \times 10^{-10})(0.13)}{(0.65 \times 10^{-3})(\sin 10.7)} \\ &= 0.869 \times 10^{-3} \text{ m} \end{aligned}$$

ii) Using Equation 23,

$$\begin{aligned} d &= \frac{4}{\pi} \cdot \frac{(\lambda)(f)}{D_e} \cdot \frac{1}{(\cos(\theta/2))} \\ &= \frac{4}{\pi} \cdot \frac{(6328 \times 10^{-10})(0.13)}{(0.65 \times 10^{-3})(\cos 10.7)} \\ &= 0.164 \times 10^{-3} \text{ m} \end{aligned}$$

iii) Using Equation 13, the fringe spacing is given by :

$$\begin{aligned}\Delta s &= \frac{\lambda}{2 \sin(\theta/2)} \\ &= \frac{6328 \times 10^{-10}}{2 \sin 10.7} \\ &= 1.70 \times 10^{-6} \text{ m}\end{aligned}$$

iv) Using Equation 24, the number of fringes in the intersecting volume is given by :

$$\begin{aligned}N_{fr} &= \frac{d}{\Delta s} \\ &= \frac{1.64 \times 10^{-4}}{1.70 \times 10^{-6}} \\ &\approx 96\end{aligned}$$

c) Using Equation 16, the local velocity measured by the velocimeter is given by :

$$\begin{aligned}\frac{U}{f_d} &= \frac{\lambda}{2 \sin(\theta/2)} \\ &= \frac{(6328 \times 10^{-10})}{2 \sin 10.7} \\ &= 1.70 \times 10^{-3} \text{ ms}^{-1}/\text{kHz}\end{aligned}$$

where f_d is measured in kHz.

- d) Size of measuring volume in relation to cross section of pore space

Consider Cell 1

Area of widest cross section
of pore space

$$= 161.29 \text{ mm}^2$$

Area of measuring volume

$$= 1.158 \text{ mm}^2$$

Fraction of pore occupied
by measuring volume

$$= \frac{1.158}{161.29}$$

$$= 0.0347$$

Appendix 2

Sample Calculation of Flow Data

Consider first data point of Cell 1

a) Flowrate,

$$\begin{aligned}
 Q &= M/p \\
 &= \frac{9.0 \times 10^{-3}}{850.1} \text{ m}^3/\text{s} \\
 &= 10.6 \text{ cc/s}
 \end{aligned}$$

b) Superficial Velocity,

$$\begin{aligned}
 q &= Q/A \\
 &= \frac{10.6}{16.42} \\
 &= 0.645 \text{ cm/s}
 \end{aligned}$$

c) Reynolds Number,

$$\begin{aligned}
 N_{rp} &= \frac{kF_b \rho q}{\mu} \\
 &= \frac{(4.7395 \times 10^{-7})(48.60)(850.1)(0.645 \times 10^{-2})}{16.4 \times 10^{-3}} \\
 &= 0.007
 \end{aligned}$$

d) Friction factor,

$$C_f = \frac{\frac{1}{F_b} \cdot \frac{\Delta p}{\Delta x}}{\rho q^2}$$

$$= \frac{\left(\frac{1}{48.60}\right)(0.34 \times 10^3)}{(850.1)(0.645 \times 10^{-2})^2}$$

$$= 198$$

Appendix 3

Table A.1 Experimental Flow Data for Cell #11

TRANSDUCER OUTPUT Volts	FLOW READING	FREQUENCY f_d , KHZ
0.11	5.4 ¹	21.8
0.23	10.1	65.0
0.42	16.1	139.
0.57	21.0	202.
0.73	21.0/20.0 ²	268.
0.86	22.8/34.0	325.
1.02	22.0/68.0	400.
1.15	22.7/85.0	440.
1.31	32.00 ³	495.
1.40	30.30	530.
1.49	28.00	565.
1.57	27.60	585.
1.65	26.30	610.
1.74	25.10	640.
1.85	23.60	665.
1.92	23.10	675.
1.95	22.85	695.
2.02	22.35	710.
2.10	21.90	720.
2.20	21.25	730.
2.50	19.90	735.
2.80	19.00	760.
3.10	18.05	
3.31	17.00	
3.56	16.55	
3.94	15.50	
4.32	14.75	
4.65	14.25	

¹ Rotameter #1² Rotameter #1/#2 connected in parallel³ Time in seconds for 5670 cc. to pass through
Trident flowmeter

Table A.2 Processed Data for Cell # 1

PRESSURE DROP $\Delta P/\Delta x$, kPa/m	Q cc/s	q cm/s	N _{rp}	C _f
0.34	10.60	0.645	0.007	198.
0.68	25.29	1.544	0.018	72.1
1.25	50.35	3.066	0.035	33.7
1.76	73.52	4.477	0.051	22.2
2.27	92.46	5.631	0.064	18.1
2.61	113.5	6.913	0.079	13.8
3.15	136.8	8.332	0.095	11.5
3.55	152.3	9.273	0.105	10.4
4.06	177.0	10.78	0.123	8.80
4.36	186.9	11.38	0.129	8.52
4.67	202.3	12.32	0.140	7.70
4.97	205.2	12.50	0.142	8.05
5.18	215.4	13.12	0.149	7.61
5.55	225.6	13.74	0.156	7.43
5.85	240.0	14.62	0.166	6.93
6.09	245.2	15.14	0.170	6.91
6.19	247.9	15.20	0.172	6.87
6.43	253.4	15.43	0.175	6.83
6.70	258.6	15.75	0.179	6.83
7.00	266.5	16.23	0.184	6.72
8.02	284.6	17.33	0.197	6.75
9.03	298.1	18.16	0.206	6.93
10.01	313.8	19.11	0.217	6.93
10.65	333.2	20.29	0.231	6.55
11.50	342.2	20.84	0.237	6.70
12.82	365.4	22.25	0.253	6.55
14.04	384.0	23.39	0.266	6.49
15.22	398.9	24.29	0.276	6.52

Table A.3 Experimental Flow Data for Cell # 2

TRANSDUCER OUTPUT Volts	FLOW READING	FREQUENCY f_d , KHZ
0.21	2.3 ¹	8.1
0.54	5.2	21.8
0.74	6.4	28.0
0.92	7.4	33.0
1.14	8.4	37.8
1.46	9.7	43.0
1.77	11.0	47.5
2.07	12.0	48.5
2.40	13.1	50.5
2.67	13.9	51.0
3.06	15.0	51.5
3.49	15.9	52.0
3.75	16.8	51.5
4.04	17.5	51.0
4.44	18.4	50.5
4.86	19.3	49.0
5.08	19.8	47.0
5.44	20.6	46.0
5.70	15.9/24.8 ²	45.5
5.88	21.4	45.0
6.04	21.8	44.5
6.50	16.0/33.8	
7.08	18.2/28.0	
7.54	17.4/36.5	
8.24	18.9/35.0	
8.95	19.2/42.5	

¹ Rotameter #1

² Rotameter #1/#2 connected in parallel

Table A.4 Processed Data for Cell # 2

PRESSURE DROP $\Delta P/\Delta x$, kPa/m	Q cc/s	q cm/s	N _{rp}	C.
0.109	3.29	0.277	0.027	43.1
0.301	9.99	0.841	0.082	12.8
0.421	13.5	1.14	0.111	9.81
0.520	16.5	1.39	0.135	8.16
0.646	21.2	1.78	0.174	6.14
0.862	24.1	2.03	0.198	6.05
1.01	28.5	2.40	0.234	5.32
1.18	32.3	2.72	0.266	4.79
1.37	36.6	3.08	0.300	4.35
1.53	40.0	3.37	0.328	4.08
1.77	44.8	3.77	0.368	3.76
2.02	49.4	4.16	0.408	3.53
2.19	53.5	4.51	0.440	3.25
2.37	56.9	4.79	0.468	3.12
2.61	61.2	5.15	0.502	2.98
2.87	65.3	5.50	0.536	2.87
3.00	67.3	5.66	0.553	2.82
3.22	71.5	6.02	0.587	2.68
3.39	73.1	6.15	0.600	2.70
3.50	75.3	6.34	0.618	2.63
3.61	77.0	6.49	0.633	2.59
3.90	81.2	6.84	0.667	2.52
4.28	86.5	7.28	0.710	2.44
4.57	90.2	7.59	0.741	2.39
5.02	96.0	8.08	0.788	2.32
5.48	103.0	8.67	0.846	2.20

Table A.5 Experimental Flow Data for Cell. # 2A

TRANSDUCER OUTPUT Volts	FLOW READING	FREQUENCY f_d , KHz
0.24	2.7 ¹	10.0
0.34	3.8	14.0
0.60	5.7	23.0
0.84	7.1	30.0
1.09	8.4	36.5
1.42	9.8	43.0
1.71	10.9	47.5
2.16	12.5	52.5
2.92	14.9	57.0
3.35	16.0	58.5
3.85	17.3	55.0
4.32	18.4	54.0
4.90	19.7	53.5
5.20	20.4	53.0
5.83	21.6	52.5
6.00	18.0/20.0 ²	52.0
6.29	22.5	
6.82	16.3/37.0	
7.61	16.2/46.5	
8.40	15.3/58.5	
8.95	15.6/64.0	

¹ Rotameter #1

² Rotameter #1/#2 connected in parallel

Table A.6 Processed Data for Cell # 2A

PRESSURE DROP $\Delta P/\Delta x$, kPa/m	Q cc/s	q cm/s	N _{rp}	C _f
0.13	4.12	0.347	0.034	33.44
0.19	6.47	0.545	0.054	19.22
0.34	11.41	0.961	0.095	11.28
0.47	15.53	1.31	0.130	8.45
0.62	19.53	1.64	0.163	7.08
0.80	24.23	2.04	0.202	5.94
0.98	28.23	2.38	0.236	5.36
1.23	34.11	2.87	0.285	4.58
1.68	44.58	3.75	0.372	3.67
1.94	49.76	4.19	0.415	3.40
2.25	55.88	4.70	0.466	3.13
2.54	61.05	5.14	0.510	2.96
2.89	67.05	5.64	0.560	2.78
3.07	70.58	5.94	0.589	2.67
3.47	76.23	6.42	0.637	2.59
3.58	78.50	6.57	0.652	2.55
3.77	80.58	6.78	0.673	2.52
4.10	85.50	7.20	0.714	2.43
4.62	93.00	7.83	0.777	2.32
5.32	98.22	8.27	0.820	2.30
5.49	104.0	8.75	0.868	2.20

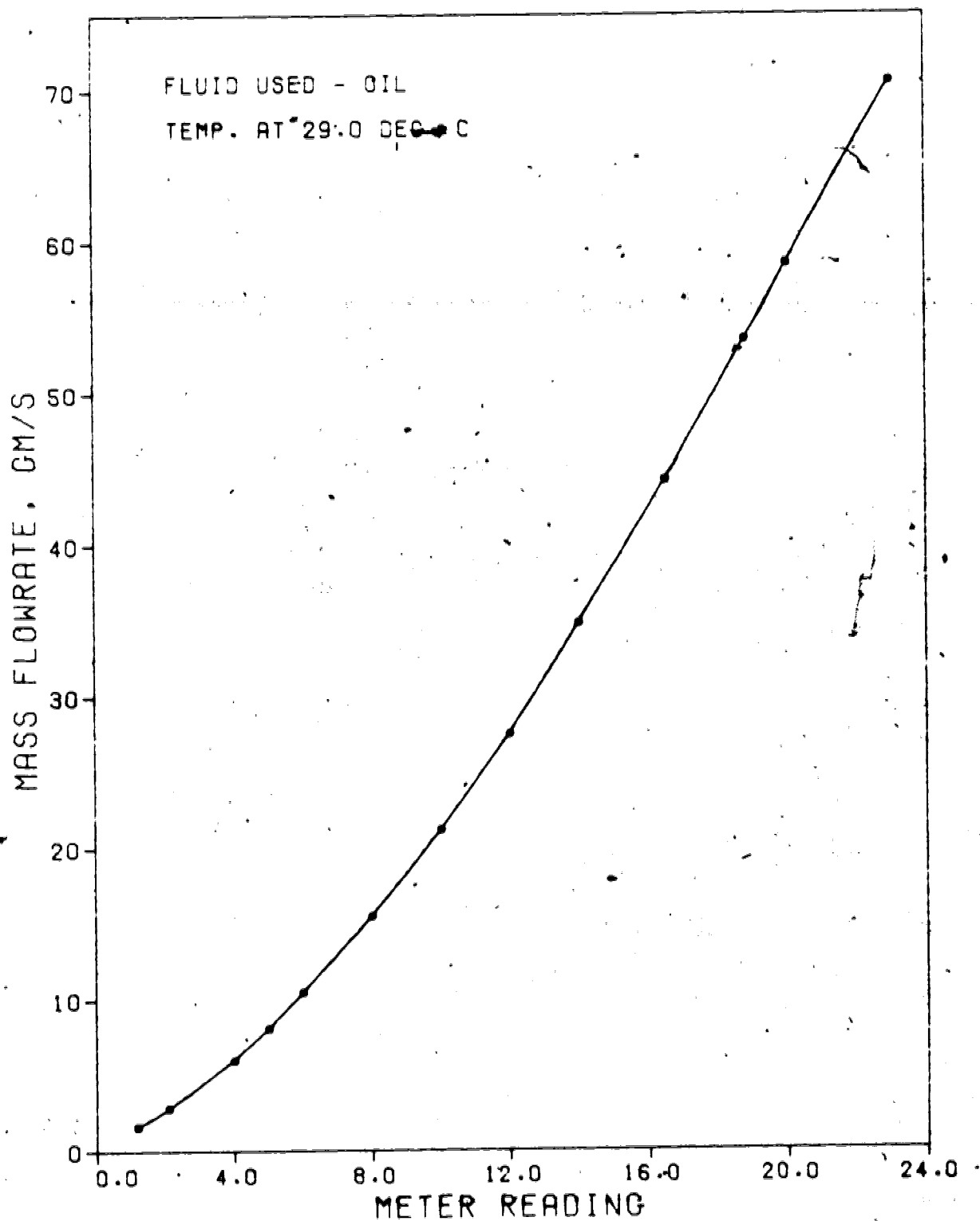


FIG. A.1 CALIBRATION CURVE FOR ROTAMETER #1

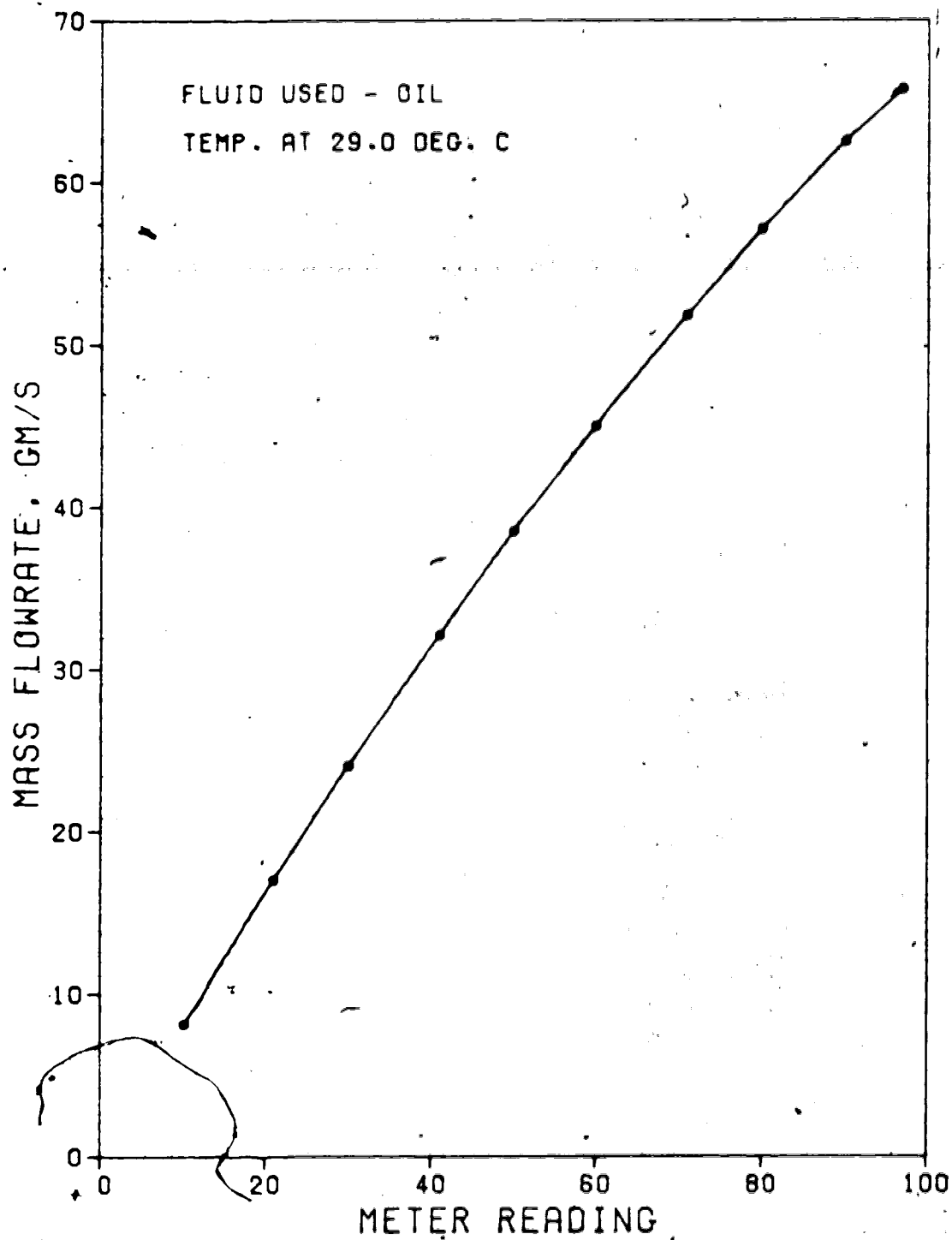


FIG: A.2 CALIBRATION CURVE FOR ROTAMETER #2

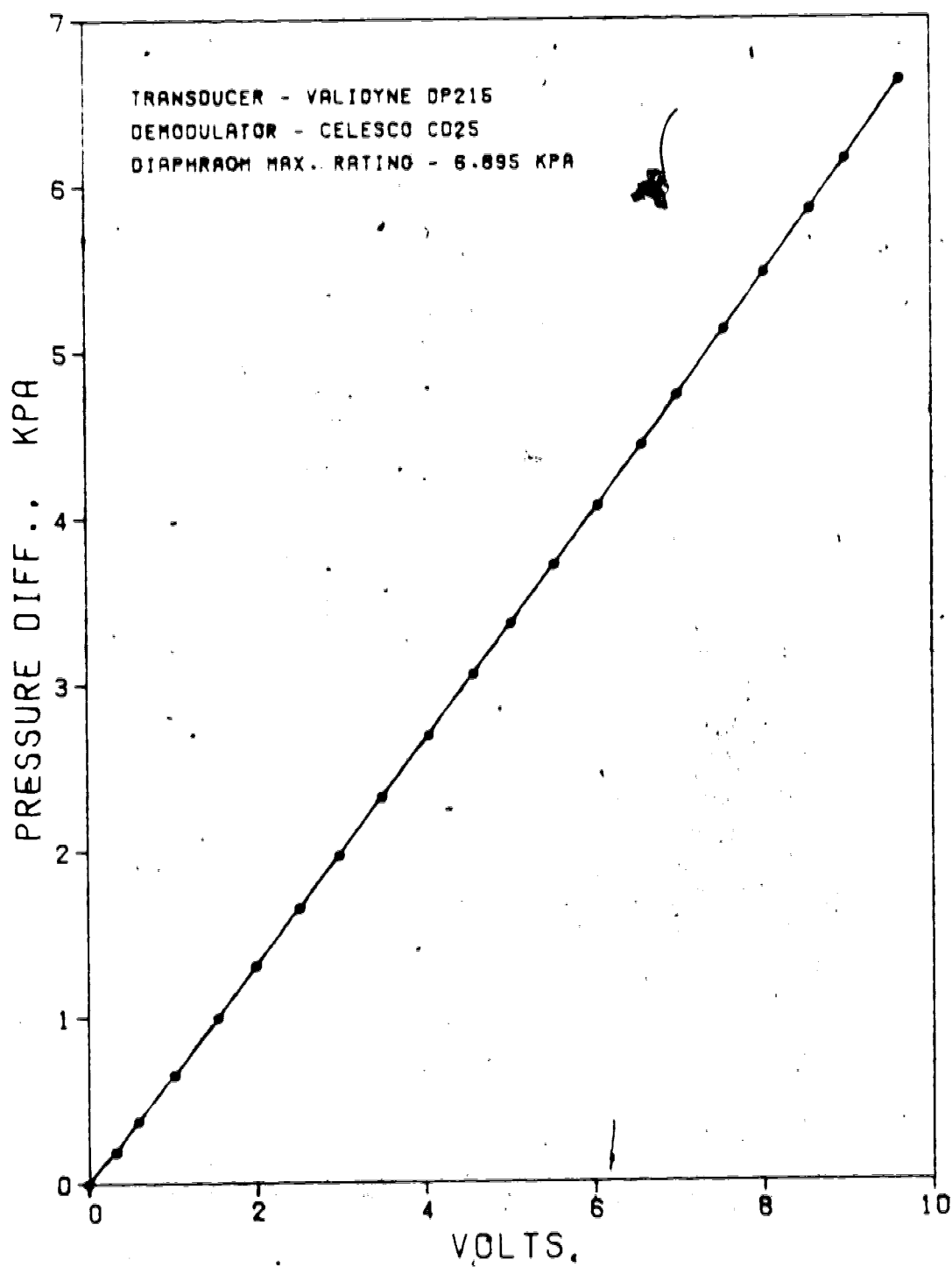


FIG. A.3 CALIBRATION GRAPH OF PRESSURE GAUGE #1

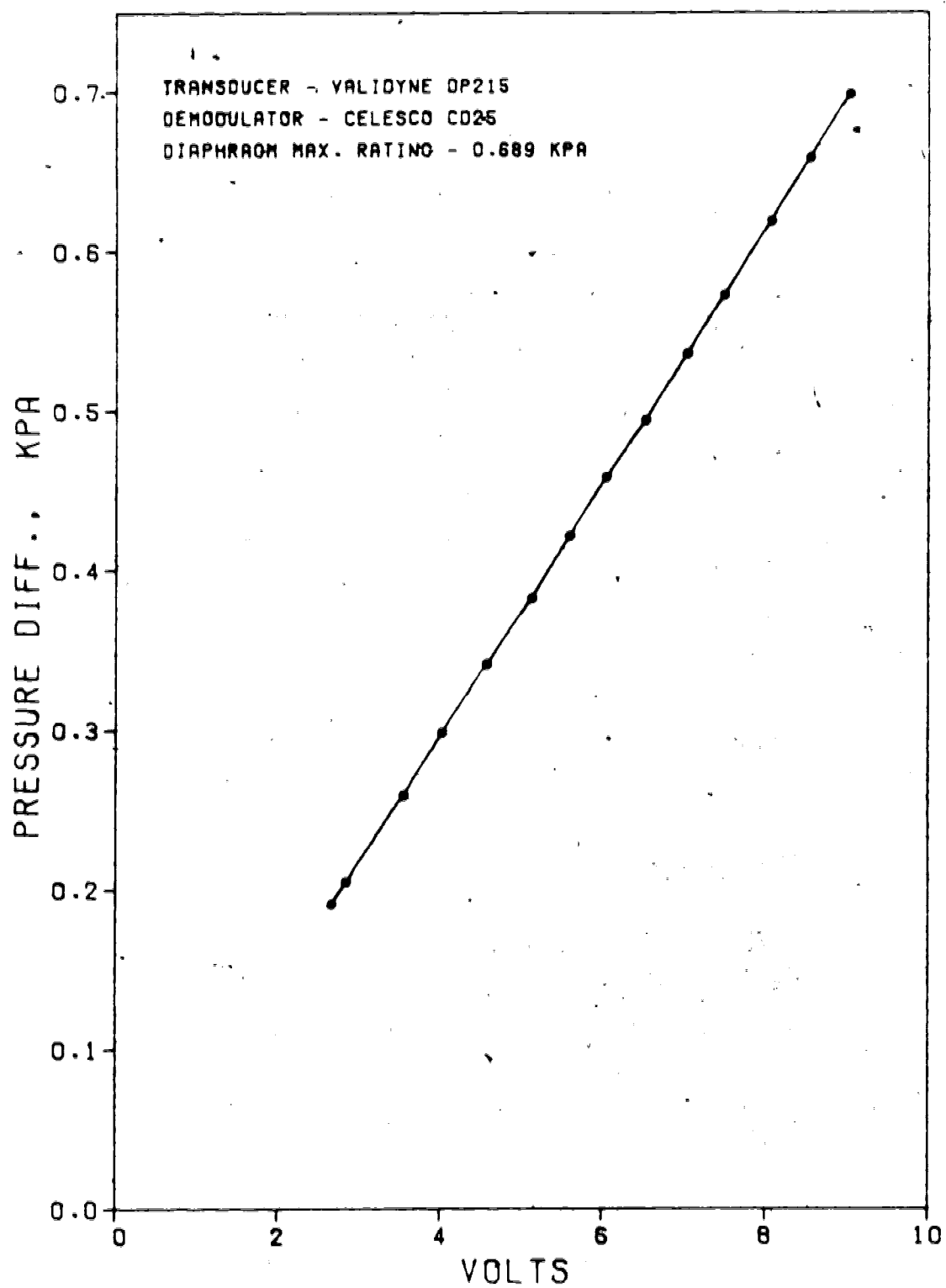


FIG. A.4 CALIBRATION GRAPH OF PRESSURE GAUGE #2